

5 The Gutzwiller Density Functional Theory

Jörg Bünemann

Computational Physics Group

BTU Cottbus

Contents

1	Introduction	2
1.1	The electronic many-particle problem	2
1.2	Density-Functional Theory (DFT)	2
1.3	Multi-Band Hubbard models	4
2	Gutzwiller wave functions	6
3	Gutzwiller energy functional in infinite dimensions	9
3.1	Diagrammatic expansion	9
3.2	Energy functional for multi-band systems	11
3.3	Example: single-band Hubbard model	15
4	Applications	16
4.1	Ferromagnetism in a Two-Band Hubbard Model	16
4.2	Antiferromagnetic order in iron-pnictide models	21
5	The Gutzwiller density-functional theory	24
5.1	The Gutzwiller DFT equations	24
5.2	Application	26
6	Summary and Outlook	27
A	Minimisation of functions with respect to non-interacting density matrices	28

1 Introduction

1.1 The electronic many-particle problem

The fundamental Hamiltonian for the electrons in solid-state theory has the well-known form ($\hbar \equiv 1$)

$$\begin{aligned} \hat{H}_{\text{el}} = & \sum_s \int d^3r \, \hat{\psi}_s^\dagger(\mathbf{r}) \left(-\frac{\Delta_{\mathbf{r}}}{2m} + V(\mathbf{r}) \right) \hat{\psi}_s(\mathbf{r}) \\ & + \frac{1}{2} \sum_{s,s'} \int d^3r \int d^3r' \, \hat{\psi}_s^\dagger(\mathbf{r}) \hat{\psi}_{s'}^\dagger(\mathbf{r}') \frac{e^2}{|\mathbf{r} - \mathbf{r}'|} \hat{\psi}_{s'}(\mathbf{r}') \hat{\psi}_s(\mathbf{r}) . \end{aligned} \quad (1)$$

In these lecture notes, we assume that the potential $V(\mathbf{r})$, generated by the atomic nuclei, is perfectly lattice periodic. The operators $\hat{\psi}_s^{(\dagger)}(\mathbf{r})$ annihilate (create) an electron at the real-space position \mathbf{r} with spin $s = \uparrow, \downarrow$. Despite the fact that the Hamiltonian (1) only describes the electronic degrees of freedom, the calculation of the electrons' properties poses a difficult many-particle problem which cannot be solved in general. The strategies to deal with the many-body problem (1) can be grouped into two main categories.

i) Model-system approaches:

In order to explain experiments, it is often sufficient to take into account only a limited number of degrees of freedom in the Hamiltonian (1). Therefore, the full problem is replaced by a simpler 'model Hamiltonian' which describes certain electronic properties of a material. Celebrated examples are the Heisenberg model for magnetic insulators and the BCS Hamiltonian for superconductors. In many-particle theory, in general, and for transition metals and their compounds, in particular, multi-band Hubbard Hamiltonians provide the standard models, see Sec. 1.3.

ii) Ab-initio approaches:

In order to cope with the full Hamiltonian (1), one has to resort to approximations which are necessarily cruder than those designed for the investigation of much simpler model systems. The most frequently used *ab-initio* approach is the 'Local-Density Approximation' (LDA) to 'Density-Functional Theory' (DFT), see Sec. 1.2.

1.2 Density-Functional Theory (DFT)

The 'Density-Functional Theory' (DFT) is based on a theorem by Hohenberg and Kohn [1]. It states that there exists a universal functional $W\{n(\mathbf{r})\}$ of the electronic density $n(\mathbf{r})$ such that

$$E\{n(\mathbf{r})\} = \int d^3r V(\mathbf{r})n(\mathbf{r}) + W\{n(\mathbf{r})\} \quad (2)$$

has its minimum, $E_0 \equiv E\{n_0(\mathbf{r})\}$, at the exact ground-state density $n_0(\mathbf{r})$ of the Hamiltonian (1) and E_0 is the corresponding ground-state energy. Since it is impossible to determine

the functional $W\{n(\mathbf{r})\}$ for many-particle systems exactly, it is necessary to develop reasonable approximations for it. Usually, one writes

$$W\{n(\mathbf{r})\} = T\{n(\mathbf{r})\} + \frac{e^2}{2} \int d^3r \int d^3r' \frac{n(\mathbf{r})n(\mathbf{r}')}{|\mathbf{r} - \mathbf{r}'|} + E_{\text{xc}}\{n(\mathbf{r})\} , \quad (3)$$

where $T\{n(\mathbf{r})\}$ is the ‘kinetic-energy functional’ and $E_{\text{xc}}\{n(\mathbf{r})\}$ is the ‘exchange-correlation functional’ which contains all Coulomb-energy contributions apart from the Hartree term that was separated in (3). Both functionals are unknown. Approximate expressions for $T\{n(\mathbf{r})\}$ and $E_{\text{xc}}\{n(\mathbf{r})\}$ are usually derived by considering a free electron gas. The kinetic energy of such electrons in the Hartree–Fock approximation is $\sim n^{5/3}$ where n is the density of the homogeneous electron gas. Therefore, a common approximation for the kinetic-energy functional in (3) is

$$T\{n(\mathbf{r})\} = \frac{3}{10m} (3\pi^2)^{2/3} \int d^3r n(\mathbf{r})^{5/3} . \quad (4)$$

In the same way, one may approximate the exchange-correlation potential in the form

$$E_{\text{xc}}\{n(\mathbf{r})\} = - \int d^3r \frac{3e^2}{4\pi} (3\pi)^{1/3} n(\mathbf{r})^{4/3} . \quad (5)$$

To work with the energy functionals (4) and (5) is a simple example of a ‘Local-Density Approximation’ (LDA) because only the local density appears in $W\{n(\mathbf{r})\}$ and corrections, e.g., involving gradients $\nabla n(\mathbf{r})$, are absent.

The DFT in LDA, as introduced so far, provides an approximate way to determine the ground-state energy and the electronic density in the ground state. These quantities are of interest if one aims, e.g., to determine the ground-state lattice structure or lattice parameters of a material. Most practical applications of the DFT, however, rely on an additional concept, the ‘Kohn–Sham scheme’. This scheme is based on the assumption that, for each system of interacting particles, there exists an effective single-particle Hamiltonian

$$\begin{aligned} \hat{H}_0^{\text{eff}} = & \sum_s \int d^3r \hat{\psi}_s^\dagger(\mathbf{r}) \left[-\frac{\Delta}{2m} + V(\mathbf{r}) \right] \hat{\psi}_s(\mathbf{r}) \\ & + \sum_s \int d^3r \hat{\psi}_s^\dagger(\mathbf{r}) \left[e^2 \int d^3r' \frac{n(\mathbf{r}')}{|\mathbf{r} - \mathbf{r}'|} + V_{\text{xc}}^{\text{KS}}\{n(\mathbf{r})\} \right] \hat{\psi}_s(\mathbf{r}) , \end{aligned} \quad (6)$$

which has the same ground-state density $n_0(\mathbf{r})$ as the original many-particle Hamiltonian (1). In general, one cannot prove rigorously that such a single-particle Hamiltonian exists; this poses the ‘ v -representability’ problem. If a system is v -representable, however, the ‘Kohn–Sham potential’ in (6) is given by

$$V_{\text{xc}}^{\text{KS}}\{n(\mathbf{r})\} = \frac{\partial}{\partial \tilde{n}(\mathbf{r})} \left(T\{\tilde{n}(\mathbf{r})\} - T'\{\tilde{n}(\mathbf{r})\} + E_{\text{xc}}\{\tilde{n}(\mathbf{r})\} \right) \Big|_{\tilde{n}(\mathbf{r})=n(\mathbf{r})} , \quad (7)$$

where $T'\{n(\mathbf{r})\}$ is the minimum kinetic energy of free non-interacting particles with the density distribution $n(\mathbf{r})$. Usually one assumes $T'\{n(\mathbf{r})\} = T\{n(\mathbf{r})\}$ such that both terms cancel each other in (7).

For our formulation of a self-consistent ‘Gutzwiller Density-Functional Theory’ (GDFT) in Sec. 5, it will be convenient to introduce a basis of local (‘Wannier’) orbitals $\phi_{i,\sigma}(\mathbf{r})$ which are centered around the L lattice sites i and carry the spin-orbital index σ . With this basis, the Hamiltonian (6) can be written as

$$\hat{H}_0^{\text{eff}} = \sum_{i,j} \sum_{\sigma,\sigma'} t_{i,j}^{\sigma,\sigma'} \{n(\mathbf{r})\} \hat{c}_{i,\sigma}^\dagger \hat{c}_{j,\sigma'} . \quad (8)$$

Here, the ‘electron transfer’ or ‘hopping’ parameters

$$t_{i,j}^{\sigma,\sigma'} \{n(\mathbf{r})\} \equiv \int d^3r \phi_{i,\sigma}^*(\mathbf{r}) \left(-\frac{\Delta \mathbf{r}}{2m} + V(\mathbf{r}) + e^2 \int d^3r' \frac{n(\mathbf{r}')}{|\mathbf{r} - \mathbf{r}'|} + V_{\text{xc}}^{\text{KS}} \{n(\mathbf{r})\} \right) \phi_{j,\sigma'}(\mathbf{r}) \quad (9)$$

depend on the particle density

$$n(\mathbf{r}) = \sum_{i,j} \sum_{\sigma,\sigma'} \phi_{i,\sigma}^*(\mathbf{r}) \phi_{j,\sigma'}(\mathbf{r}) \langle \hat{c}_{i,\sigma}^\dagger \hat{c}_{j,\sigma'} \rangle_{\Psi_0} , \quad (10)$$

where $|\Psi_0\rangle$ is the ground state of (8),

$$\hat{H}_0^{\text{eff}} |\Psi_0\rangle = E_0 |\Psi_0\rangle . \quad (11)$$

At least in principle, the self-consistent solution of the ‘Kohn–Sham equations’ (8)-(11) is the central part of most DFT applications in solid-state physics. Note, however, that actual numerical implementations of the DFT usually do not work with Wannier functions but use atomic orbitals or plane waves as basis sets.

Despite the rather drastic approximations which have led to the Kohn–Sham equations, a comparison of theoretical and experimental results has revealed a remarkable agreement for a large number of materials. Therefore, the LDA has become the most important tool for the investigation of electronic properties in solid-state physics. There are, however, well-known problems with certain classes of materials. For example, band gaps in insulators or semiconductors are usually found to be significantly smaller in DFT than in experiment. Even bigger discrepancies arise for materials with strong local Coulomb interactions. These are, in particular, transition metals, lanthanides, and their respective compounds. Such systems have been investigated in the past mostly based on model systems, which we discuss in the following section.

1.3 Multi-Band Hubbard models

We distinguish ‘localised’ orbitals, $\sigma \in \ell$, and ‘delocalised’ orbitals, $\sigma \in d$, where the localised orbitals are those which require a more sophisticated treatment of the local Coulomb interaction than provided by the LDA. The natural starting point for such a treatment is a multi-band Hubbard model of the form

$$\hat{H}_H = \hat{H}_0 + \sum_i \hat{H}_{i;c} , \quad (12)$$

$$\hat{H}_0 \equiv \sum_{i \neq j} \sum_{\sigma,\sigma'} t_{i,j}^{\sigma,\sigma'} \hat{c}_{i,\sigma}^\dagger \hat{c}_{j,\sigma'} + \sum_i \sum_{\sigma,\sigma' \in d} \epsilon_i^{\sigma,\sigma'} \hat{c}_{i,\sigma}^\dagger \hat{c}_{i,\sigma'} , \quad (13)$$

$$\hat{H}_{i;c} \equiv \sum_{\sigma,\sigma' \in \ell} \epsilon_i^{\sigma,\sigma'} \hat{c}_{i,\sigma}^\dagger \hat{c}_{i,\sigma'} + \sum_{\sigma_1,\sigma_2,\sigma_3,\sigma_4 \in \ell} U_i^{\sigma_1,\sigma_2,\sigma_3,\sigma_4} \hat{c}_{i,\sigma_1}^\dagger \hat{c}_{i,\sigma_2}^\dagger \hat{c}_{i,\sigma_3} \hat{c}_{i,\sigma_4} . \quad (14)$$

#	Atomic eigenstate $ \Gamma\rangle$	Symmetry	energy E_Γ
1	$ \uparrow, \uparrow\rangle$	3A_2	$U' - J$
2	$(\uparrow, \downarrow\rangle + \downarrow, \uparrow\rangle)/\sqrt{2}$	3A_2	$U' - J$
3	$ \downarrow, \downarrow\rangle$	3A_2	$U' - J$
4	$(\uparrow, \downarrow\rangle - \downarrow, \uparrow\rangle)/\sqrt{2}$	1E	$U' + J$
5	$(\uparrow\downarrow, 0\rangle - 0, \uparrow\downarrow\rangle)/\sqrt{2}$	1E	$U - J_C$
6	$(\uparrow\downarrow, 0\rangle + 0, \uparrow\downarrow\rangle)/\sqrt{2}$	1A_1	$U + J_C$

Table 1: Two-particle eigenstates with symmetry specifications and energies.

This model contains a general two-particle interaction in the localised orbitals, and fixed hopping parameters, $t_{i,j}^{\sigma,\sigma'}$, and orbital energies, $\epsilon_i^{\sigma,\sigma'} = t_{i,i}^{\sigma,\sigma'}$. Since the parameters $t_{i,j}^{\sigma,\sigma'}$ are usually derived from a DFT calculation, see Eq. (9), they already contain the Coulomb interaction on a DFT level. For the localised orbitals this means that, through the on-site energies $\epsilon_i^{\sigma,\sigma'}$, the Coulomb interaction appears twice in the Hamiltonian $\hat{H}_{i;c}$. We will address this so-called ‘double-counting problem’ in Sec. 5.

In the context of the Gutzwiller variational theory we need the eigenstates $|\Gamma\rangle_i$ and the eigenvalues $E_{i,\Gamma}$ of the Hamiltonian $\hat{H}_{i;c}$. They allow us to write $\hat{H}_{i;c}$ as

$$\hat{H}_{i;c} = \sum_{\Gamma} E_{i,\Gamma} \hat{m}_{i,\Gamma} \quad , \quad \hat{m}_{i,\Gamma} \equiv |\Gamma\rangle_i \langle \Gamma| \quad . \quad (15)$$

As a simple example, we consider a model with two degenerate e_g orbitals in a cubic environment. In this case, we may set $\epsilon_i^{\sigma,\sigma'} = 0$ and the local Hamiltonian then has the form

$$\begin{aligned} \hat{H}_{i;c} = & U \sum_e \hat{n}_{e,\uparrow} \hat{n}_{e,\downarrow} + U' \sum_{s,s'} \hat{n}_{1,s} \hat{n}_{2,s'} - J \sum_s \hat{n}_{1,s} \hat{n}_{2,s} \\ & + J \sum_s \hat{c}_{1,s}^\dagger \hat{c}_{2,s}^\dagger \hat{c}_{1,\bar{s}} \hat{c}_{2,s} + J_C \left(\hat{c}_{1,\uparrow}^\dagger \hat{c}_{1,\downarrow}^\dagger \hat{c}_{2,\downarrow} \hat{c}_{2,\uparrow} + \hat{c}_{2,\uparrow}^\dagger \hat{c}_{2,\downarrow}^\dagger \hat{c}_{1,\downarrow} \hat{c}_{1,\uparrow} \right) , \end{aligned} \quad (16)$$

where $e = 1, 2$ labels the e_g orbitals, $s = \uparrow, \downarrow$ is the spin index and we use the convention $\bar{\uparrow} \equiv \downarrow$, $\bar{\downarrow} \equiv \uparrow$. For e_g orbitals, only two of the three parameters in (16) are independent since the symmetry relations $U' = U - 2J$ and $J = J_C$ hold. In our model, we have four spin-orbital states $\sigma = (e, s)$ per atom, leading to a $2^4 = 16$ -dimensional atomic Hilbert space. All eigenstates $|\Gamma\rangle_i$ of $\hat{H}_{i;c}$ with particle numbers $N \neq 2$ are simple Slater determinants of spin-orbital states $|\sigma\rangle$ and their energies are

$$\begin{aligned} E_\Gamma &= 0 & (N = 0, 1) , \\ E_\Gamma &= U + 2U' - J & (N = 3) , \\ E_\Gamma &= 2U + 4U' - 2J & (N = 4) . \end{aligned} \quad (17)$$

The two-particle eigenstates are slightly more complicated because some of them are linear combinations of Slater determinants. We introduce the basis

$$|s, s'\rangle \equiv \hat{c}_{1,s}^\dagger \hat{c}_{2,s'}^\dagger |0\rangle \quad , \quad |\uparrow\downarrow, 0\rangle \equiv \hat{c}_{1,\uparrow}^\dagger \hat{c}_{1,\downarrow}^\dagger |0\rangle \quad , \quad |0, \uparrow\downarrow\rangle \equiv \hat{c}_{2,\uparrow}^\dagger \hat{c}_{2,\downarrow}^\dagger |0\rangle \quad (18)$$

of two-particle states, which are used to set up the eigenstates of $\hat{H}_{i;c}$, see table 1. The states of lowest energy are the three triplet states with spin $S = 1$, which belong to the representation A_2 of the cubic point-symmetry group. Finding a high-spin ground state is a simple consequence of Hund's first rule. Higher in energy are the two degenerate singlet states of symmetry E and the non-degenerate singlet state of symmetry A_1 .

The eigenstates of the local Hamiltonian $\hat{H}_{i;c}$ play an essential role in the formulation of the multi-band Gutzwiller theory in Sec. 2. Since in most applications only a finite (and not too large) number of localised orbitals is taken into account, these eigenstates can be readily calculated by standard numerical techniques. The special case of a $3d$ -shell in a cubic environment has been discussed analytically in great detail in the textbook by Sugano, Ref. [2].

2 Gutzwiller wave functions

The single-band Hubbard model

To understand the main physical idea behind the Gutzwiller variational theory it is instructive to start with a consideration of the single-band Hubbard model

$$\hat{H}_{1B} = \sum_{i,j} \sum_{s=\uparrow,\downarrow} t_{i,j} \hat{c}_{i,s}^\dagger \hat{c}_{j,s} + U \sum_i \hat{d}_i, \quad \hat{d}_i \equiv \hat{n}_{i,\uparrow} \hat{n}_{i,\downarrow}. \quad (19)$$

In Hartree–Fock theory, one uses a variational wave function which is a one-particle product state

$$|\Psi_0\rangle = \prod_{\gamma} \hat{h}_{\gamma}^\dagger |0\rangle. \quad (20)$$

in order to investigate many-particle Hamiltonians such as (19). It is well known, however, that such wave functions are insufficient for systems with medium to strong Coulomb interaction effects, see, e.g. our later discussion in Sec. 4. It is a particular problem of a Hartree–Fock treatment that local charge fluctuations can only be suppressed in that approach by a spurious breaking of symmetries. Therefore, it usually overestimates the stability of phases with a broken symmetry. Hartree–Fock wave functions, however, can still be a reasonable starting point in order to set up more sophisticated variational wave functions. This leads us to the general class of ‘Jastrow wave functions’ [3, 4], which are defined as

$$|\Psi_J\rangle = \hat{P}_J |\Psi_0\rangle. \quad (21)$$

Here, $|\Psi_0\rangle$ is again a one-particle product state and \hat{P}_J is a correlation operator, which can be chosen in various ways in order to minimise the variational ground-state energy. The ‘Gutzwiller wave function’ (GWF) is a special Jastrow wave function with a particular choice of the correlation operator \hat{P}_J . It was introduced by Gutzwiller [5–7] in the form

$$|\Psi'_G\rangle \equiv \hat{P}'_G |\Psi_0\rangle = \prod_i \hat{P}'_i |\Psi_0\rangle \quad (22)$$

and with the purpose to study ferromagnetism in a single-band Hubbard model. The (local) ‘Gutzwiller correlation operator’

$$\hat{P}'_i \equiv g^{\hat{d}_i} = 1 - (1 - g)\hat{d}_i, \quad (23)$$

for each lattice site i contains a variational parameter g (with $0 \leq g \leq 1$), which allows one to suppress local double occupancies that are energetically unfavourable for a finite Hubbard interaction $U > 0$.

The Hilbert space of the local Hamiltonian for the one-band Hubbard model is four-dimensional where a local basis $|I\rangle$ is given by the states $|\emptyset\rangle$, $|\uparrow\rangle$, $|\downarrow\rangle$, and $|d\rangle$ for empty, singly-occupied and doubly-occupied sites, respectively. By working with the occupation operator \hat{d}_i in (23), Gutzwiller singled out the doubly-occupied state $|d\rangle$. A more symmetric definition of the *local* Gutzwiller correlator (23) is given by

$$\hat{P}_i = \prod_I \lambda_I^{\hat{m}_{i,I}} = \sum_I \lambda_I \hat{m}_{i,I} \quad (24)$$

where the operators $\hat{m}_{i,I} = |I\rangle_i \langle I|$ are the projectors onto the four atomic eigenstates $|I\rangle$. The operator (24) contains four parameters λ_I instead of only one parameter g in Gutzwiller’s definition (23). It can be readily shown, however, that the operators (23) and (24) define the same sets of variational wave functions as long as the respective one-particle states $|\Psi_0\rangle$ are also treated as variational objects. Therefore, the wave functions, defined by (24), contain more variational parameters than are actually needed. This surplus of parameters will turn out to be quite useful when we evaluate expectation values in the limit of infinite spatial dimensions. Moreover, for the multi-band generalisation of Gutzwiller wave functions in the following section, Eq. (24) is the most natural starting point.

Multi-band Hubbard models

It is pretty obvious [8, 9] how the Gutzwiller wave functions (22) can be generalised for the investigation of the multi-band Hubbard models (12). The starting point is again a (normalised) single-particle product state $|\Psi_0\rangle$ to which we apply a Jastrow factor that is a product of local correlation operators. Hence, the multi-band Gutzwiller wave functions are given as

$$|\Psi_G\rangle = \hat{P}_G |\Psi_0\rangle = \prod_i \hat{P}_i |\Psi_0\rangle, \quad (25)$$

where, as in (24), we might work with a local correlation operator of the form

$$\hat{P}_i = \sum_{\Gamma_i} \lambda_{i;\Gamma_i} \hat{m}_{i;\Gamma_i}, \quad \hat{m}_{i;\Gamma_i} = |\Gamma\rangle_i \langle \Gamma|. \quad (26)$$

The variational parameters $\lambda_{i;\Gamma_i}$ allow us to optimise the occupation of each eigenstate $|\Gamma\rangle$ of the local Hamiltonian $\hat{H}_{i;c}$. In multi-orbital systems, however, these states are usually degenerate and not uniquely defined. Moreover, it is not clear whether, in a solid, the (atomic) eigenstates

$|\Gamma\rangle_i$ lead to the best variational ground state of the form (25). Instead of (26) it may therefore be better to work with the general local correlation operator

$$\hat{P}_i = \sum_{\Gamma_i, \Gamma'_i} \lambda_{i; \Gamma_i, \Gamma'_i} |\Gamma\rangle_i \langle \Gamma'| \quad , \quad (27)$$

which contains a matrix $\lambda_{i; \Gamma_i, \Gamma'_i}$ of variational parameters. The analytical evaluation of expectation values, which we discuss in the following section, can be carried out without additional efforts for the general correlation operator (27). In numerical applications, however, we often have to restrict ourself to the simpler operator (26) since the number of parameters $\lambda_{i; \Gamma_i, \Gamma'_i}$ may become prohibitively large. Alternatively, one can try to identify the ‘relevant’ non-diagonal elements of $\lambda_{i; \Gamma_i, \Gamma'_i}$ and take only these into account. Such strategies have been discussed in more detail in Ref. [10].

For systems without superconductivity, the Gutzwiller wave function should be an eigenstate of the total particle number operator

$$\hat{N} = \sum_{i, \sigma} \hat{n}_{i, \sigma} \quad . \quad (28)$$

This requires that \hat{N} commutes with \hat{P}_G , which leads to

$$\sum_{\Gamma, \Gamma'} \lambda_{i; \Gamma, \Gamma'} (|\Gamma| - |\Gamma'|) |\Gamma\rangle_i \langle \Gamma'| = 0 \quad (29)$$

where $|\Gamma|$ is the number of particles in the state $|\Gamma\rangle_i$. From equation (29), we conclude that $\lambda_{i; \Gamma, \Gamma'}$ can only be finite for states $|\Gamma\rangle_i, |\Gamma'\rangle_i$ with the same particle number. In a similar way, one can show that these states have to belong to the same representation of the point symmetry group. To study superconducting systems, one works with BCS-type one-particle wave functions $|\Psi_0\rangle$ for which the particle number is not conserved. In this case, the variational-parameter matrix $\lambda_{i; \Gamma, \Gamma'}$ has to be finite also for states $|\Gamma\rangle_i, |\Gamma'\rangle_i$ with different particle numbers, see Refs. [9, 11].

To keep notations simple in this tutorial presentation, we will restrict ourself to the case of a diagonal and real variational-parameter matrix and do not consider superconducting states. Consequently, the local correlation operators are Hermitian, $\hat{P}_i^\dagger = \hat{P}_i$. Moreover, we work with a spin-orbital basis σ for which the non-interacting local density matrix

$$C_{i; \sigma, \sigma'} \equiv \langle \hat{c}_{i, \sigma}^\dagger \hat{c}_{i, \sigma'} \rangle_{\Psi_0} \quad (30)$$

is diagonal,

$$C_{i; \sigma, \sigma'} = \delta_{\sigma, \sigma'} n_{i, \sigma}^0 \quad . \quad (31)$$

This can always be achieved (i.e., for any $|\Psi_0\rangle$) by a proper transformation of the local basis σ . To simplify the notations further, we will frequently drop lattice-site indices in purely local equations.

3 Gutzwiller energy functional in infinite dimensions

The evaluation of expectation values for Gutzwiller wave functions remains a difficult many-particle problem even in the simplest case of a single-band Hubbard model. It has been achieved for this model in one dimension both for paramagnetic and for ferromagnetic states [12–16]. In the opposite limit of infinite spatial dimensions, expectation values can be evaluated for the general class of wave-functions (25). In this section, we summarise the main technical ideas behind this evaluation and discuss the resulting energy functional. An application of this functional to finite-dimensional systems is usually denoted as the ‘Gutzwiller approximation’ because, for the single-band model, Gutzwiller has derived the very same functional [5–7] by means of combinatorial techniques [17].

3.1 Diagrammatic expansion

In order to determine the expectation value

$$\langle \hat{H}_H \rangle_{\Psi_G} = \frac{\langle \Psi_G | \hat{H}_H | \Psi_G \rangle}{\langle \Psi_G | \Psi_G \rangle} \quad (32)$$

of the Hamiltonian (12) we need to evaluate the following quantities ($i \neq j$)

$$\langle \Psi_G | \hat{c}_{i,\sigma}^\dagger \hat{c}_{j,\sigma'} | \Psi_G \rangle = \left\langle (\hat{P}_i \hat{c}_{i,\sigma}^\dagger \hat{P}_i) (\hat{P}_j \hat{c}_{j,\sigma'} \hat{P}_j) \prod_{l \neq (i,j)} \hat{P}_l^2 \right\rangle_{\Psi_0}, \quad (33)$$

$$\langle \Psi_G | \hat{m}_{i,\Gamma} | \Psi_G \rangle = \left\langle (\hat{P}_i \hat{m}_{i,\Gamma} \hat{P}_i) \prod_{l \neq i} \hat{P}_l^2 \right\rangle_{\Psi_0}, \quad (34)$$

$$\langle \Psi_G | \Psi_G \rangle = \left\langle \prod_l \hat{P}_l^2 \right\rangle_{\Psi_0}. \quad (35)$$

The r.h.s. of all three equations (33)-(35) can be evaluated by means of Wick’s theorem because the wave function $|\Psi_0\rangle$ is a single-particle product state. In this way, we can represent all contributions by diagrams with ‘internal vertices’ l (from operators \hat{P}_l^2), ‘external vertices’ i in Eq. (34) (or i and j in Eq. (33)) and lines

$$P_{l,l'}^{\sigma,\sigma'} \equiv \langle \hat{c}_{l,\sigma}^\dagger \hat{c}_{l',\sigma'} \rangle_{\Psi_0} \quad (36)$$

which connect these vertices. This diagrammatic expansion, however, is still very complicated even in the limit of infinite spatial dimensions. As shown in more detail in Refs. [8,9], it is very beneficial in this limit to introduce the (local) constraints

$$1 = \langle \hat{P}_l^2 \rangle_{\Psi_0}, \quad (37)$$

$$\langle \hat{c}_{l,\sigma}^\dagger \hat{c}_{l,\sigma'} \rangle_{\Psi_0} = \langle \hat{c}_{l,\sigma}^\dagger \hat{P}_l^2 \hat{c}_{l,\sigma'} \rangle_{\Psi_0}. \quad (38)$$

These constraints do not restrict our total set of variational wave functions (25) because they merely exploit the fact that we have introduced more variational parameters λ_Γ than are actually

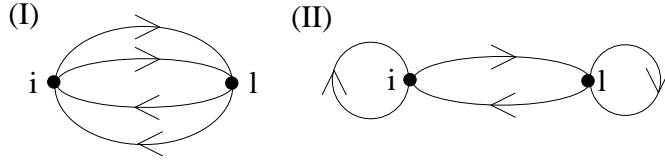


Fig. 1: Two examples of double-occupancy diagrams ($l \neq i$). Diagram (II) vanishes due to the constraints (37), (38). Diagram (I) vanishes in the limit of infinite spatial dimensions.

needed; see the discussion on the single-band model in Sec. 2. Note that moving the operator \hat{P}_l^2 relative to $\hat{c}_{l,\sigma}^\dagger$ and $\hat{c}_{l,\sigma'}$ does not alter the whole set of constraints (37), (38).

The constraints (37), (38) have an important consequence: Each diagram that results from (33)-(35) is non-zero only when all of its internal vertices l are connected to other vertices by at least four lines. As a simple example, Fig. 1 shows two (first order) diagrams which result from (34). While the constraints do not affect diagram (I), they ensure that diagram (II) vanishes.

In order to have a meaningful (i.e., finite) kinetic energy per lattice site our lines have to vanish like

$$P_{i,j}^{\sigma,\sigma'} \sim \frac{1}{\sqrt{2D}^{\|i-j\|}}, \quad (39)$$

on a hyper-cubic lattice in the limit of large spatial dimensions D . Here, we introduced the ‘New-York metric’

$$\|i-j\| \equiv \sum_{k=1}^D |R_{i,k} - R_{j,k}|, \quad (40)$$

where $R_{i,k}$ is the k -th component of the lattice site vector \mathbf{R}_i . Note that the number of neighbouring sites with distance $\|i-j\|$ is given by

$$N_{\text{n.n.}}^{\|i-j\|} = 2D^{\|i-j\|}. \quad (41)$$

The scaling behaviour (39) in infinite dimensions has significant consequences for our diagrammatic expansion. As an example, we consider diagram (I) in Fig. 1. If we skip, for simplicity, any spin-orbital dependence of lines, this diagram leads to the contribution

$$\text{diagram (I)} \sim \sum_l P_{i,l}^4 = \mathcal{O}\left(\frac{1}{D}\right) \xrightarrow{D \rightarrow \infty} 0. \quad (42)$$

where the scaling $1/D$ results from equations (39) and (41). In general, one can show that in infinite dimensions a diagram vanishes if it contains an internal vertex that is connected to other vertices by three or more lines. The constraints (37), (38) ensure that this is the case for *all* diagrams which contain at least one internal vertex. Our arguments, so far, only apply to diagrams in which all internal vertices are connected to the external vertices i (or i and j). Of course, if we apply Wick’s theorem to equations (33)-(34) we also obtain diagrams with internal vertices that are not connected to the external vertices. These diagrams, however, are exactly cancelled by the norm diagrams from Eq. (35) as shown in Ref. [8]. In summary, we therefore end up with the simple results

$$\langle \hat{c}_{i,\sigma}^\dagger \hat{c}_{j,\sigma'} \rangle_{\Psi_G} = \left\langle (\hat{P}_i \hat{c}_{i,\sigma}^\dagger \hat{P}_i) (\hat{P}_j \hat{c}_{j,\sigma'} \hat{P}_j) \right\rangle_{\Psi_0}, \quad (43)$$

$$\langle \hat{m}_{i;\Gamma} \rangle_{\Psi_G} = \left\langle (\hat{P}_i \hat{m}_{i;\Gamma} \hat{P}_i) \right\rangle_{\Psi_0}, \quad (44)$$

for expectation values in the limit of infinite spatial dimensions. These expectation values and the constraints (37), (38) will be further analysed in the following section and lead us to the Gutzwiller energy functional in infinite dimensions.

3.2 Energy functional for multi-band systems

Notations

We assume that the $2N$ (localised) spin-orbital states σ are ordered in some arbitrary way, $\sigma = 1, \dots, 2N$ where N is the number of localised orbitals per lattice site. In order to set up a proper basis of the local Hilbert space which belongs to $\hat{H}_{i;c}$, we introduce the following notations for the 2^{2N} possible electronic configurations ('Slater determinants').

- i) An atomic configuration I is characterised by the electron occupation of the orbitals,

$$I \in \{\emptyset; (1), \dots, (2N); (1, 2), \dots, (2, 3), \dots, (2N-1, 2N); \dots; (1, \dots, 2N)\}, \quad (45)$$

where the elements in each set $I = (\sigma_1, \sigma_2, \dots)$ are ordered, i.e., it is $\sigma_1 < \sigma_2 < \dots$. In general, we interpret the indices I as sets in the usual mathematical sense. For example, in the atomic configuration $I \setminus I'$ only those orbitals in I that are not in I' are occupied. The 'complement' \bar{I} is defined as

$$\bar{I} \equiv (1, \dots, 2N) \setminus I. \quad (46)$$

where $(1, \dots, 2N)$ is the state with the maximum number of $2N$ electrons.

- ii) A state with a specific configuration I is given as

$$|I\rangle = \hat{C}_I^\dagger |0\rangle \equiv \prod_{\sigma \in I} \hat{c}_\sigma^\dagger |0\rangle = \hat{c}_{\sigma_1}^\dagger \dots \hat{c}_{\sigma_{|I|}}^\dagger |0\rangle, \quad (47)$$

where the operators \hat{c}_σ^\dagger are in ascending order, i.e., it is $\sigma_1 < \sigma_2 < \dots < \sigma_{|I|}$ and $|I|$ is the number of particles in I . Products of annihilation operators, such as

$$\hat{C}_I \equiv \prod_{\sigma \in I} \hat{c}_\sigma = \hat{c}_{\sigma_1} \dots \hat{c}_{\sigma_{|I|}}, \quad (48)$$

will be placed in descending order, i.e., with $\sigma_1 > \sigma_2 > \dots > \sigma_{|I|}$. Note that we have introduced the operators \hat{C}_I^\dagger and \hat{C}_I just as convenient abbreviations. They must not be misinterpreted as fermionic creation or annihilation operators. The 'sign function'

$$f(\sigma, I) \equiv \langle I \cup \sigma | \hat{c}_\sigma^\dagger | I \rangle \quad (49)$$

counts whether an odd or even number of commutations is required to place σ in its proper position in I ($f(\sigma, I) = \mp 1$). It vanishes if $\sigma \in I$.

- iv) The operator $\hat{m}_{I,I'} \equiv |I\rangle \langle I'|$ describes the transfer between configurations I' and I . It can be written as

$$\hat{m}_{I,I'} = \hat{C}_I^\dagger \hat{C}_{I'} \prod_{\sigma'' \in J} (1 - \hat{n}_{\sigma''}) \quad (50)$$

where $J \equiv \overline{I \cup I'}$. A special case, which derives from (50), is the occupation operator

$$\hat{m}_I \equiv |I\rangle \langle I| = \prod_{\sigma \in I} \hat{n}_\sigma \prod_{\sigma' \in \bar{I}} (1 - \hat{n}_{\sigma'}) . \quad (51)$$

The states $|I\rangle$ form a basis of the atomic Hamiltonian's Hilbert space. Therefore, we can write the eigenstates of the local Hamiltonian (15) as

$$|\Gamma\rangle = \sum_I T_{I,\Gamma} |I\rangle \quad (52)$$

with coefficients $T_{I,\Gamma}$. For a simple example, see the two-particle states in table 1.

Local energy

The evaluation of the r.h.s. of Eq. (44) is straightforward if we use

$$\hat{P} \hat{m}_\Gamma \hat{P} = \lambda_\Gamma^2 \hat{m}_\Gamma . \quad (53)$$

This equation gives us

$$\langle \hat{m}_\Gamma \rangle_{\Psi_G} = \lambda_\Gamma^2 m_\Gamma^0 , \quad (54)$$

where

$$m_\Gamma^0 = \langle \hat{m}_\Gamma \rangle_{\Psi_0} = \sum_I |T_{I,\Gamma}|^2 m_I^0 , \quad m_I^0 = \prod_{\sigma \in I} n_\sigma^0 \prod_{\sigma \notin I} (1 - n_\sigma^0) . \quad (55)$$

Here we have used Eqs. (26), (31), and (51).

Hopping expectation values

For the evaluation of (43) we start with

$$\hat{P} \hat{c}_\sigma^\dagger \hat{P} = \sum_{\Gamma, \Gamma'} \lambda_\Gamma \lambda_{\Gamma'} \sum_{I_1, I'_1, I_2, I'_2} \langle I_2 | \hat{c}_\sigma^\dagger | I'_1 \rangle T_{I_1, \Gamma} T_{I_2, \Gamma}^* T_{I'_1, \Gamma'} T_{I'_2, \Gamma'}^* \hat{m}_{I_1, I'_2} \quad (56)$$

which follows from Eqs. (26), (50), (52). Note that the second operator $\hat{P} \hat{c}_{\sigma'} \hat{P}$ in (43) is just the conjugate of (56) with σ replaced by σ' . Hence, the only remaining expectation values which we need to evaluate in (43) have the form

$$E(I, I'; J, J') \equiv \langle \hat{m}_{i; I, I'} \hat{m}_{j; J, J'} \rangle_{\Psi_0} . \quad (57)$$

An application of Wick's Theorem to (57) leads, in general, to a number of diagrams with (potentially) several lines connecting the lattice sites i and j . At this point, however, we again apply the infinite-dimensional rule that all diagrams with three or more lines connecting i and j

can be discarded. Hence, the only remaining diagrams are those with exactly one line between i and j . Together with Eq. (31), we therefore find

$$E(I, I'; J, J') = \sum_{\gamma} f(\gamma, I') \delta_{I, I' \cup \gamma} \frac{m_{I'}^0}{1 - n_{\gamma}^0} \sum_{\gamma'} f(\gamma', J) \delta_{J \cup \gamma', J'} \frac{m_J^0}{1 - n_{\gamma'}^0} \langle \hat{c}_{i, \gamma}^{\dagger} \hat{c}_{j, \gamma'} \rangle_{\Psi_0} . \quad (58)$$

Altogether, we obtain the following result for the hopping expectation value (43) in infinite dimensions

$$\langle \hat{c}_{i, \sigma}^{\dagger} \hat{c}_{j, \sigma'} \rangle_{\Psi_G} = \sum_{\gamma, \gamma'} q_{\sigma}^{\gamma} q_{\sigma'}^{\gamma'} \langle \hat{c}_{i, \gamma}^{\dagger} \hat{c}_{j, \gamma'} \rangle_{\Psi_0} \quad (59)$$

with the ‘renormalisation matrix’

$$q_{\sigma}^{\gamma} = \frac{1}{1 - n_{\gamma}^0} \sum_{\Gamma, \Gamma'} \lambda_{\Gamma} \lambda_{\Gamma'} \sum_{I, I'} f(\sigma, I) f(\gamma, I') T_{I \cup \sigma, \Gamma}^* T_{I, \Gamma'} T_{I', \Gamma'}^* T_{I' \cup \gamma, \Gamma} m_{I'}^0 \quad (60)$$

$$= \frac{1}{n_{\gamma}^0} \sum_{\Gamma, \Gamma'} \lambda_{\Gamma} \lambda_{\Gamma'} \langle \Gamma | \hat{c}_{\sigma}^{\dagger} | \Gamma' \rangle \left\langle (| \Gamma \rangle \langle \Gamma' | \hat{c}_{\gamma}) \right\rangle_{\Psi_0} . \quad (61)$$

Constraints

The explicit form of the correlation operator (26), together with Eq. (31), gives us directly the explicit form of the constraints (37), (38)

$$1 = \sum_{\Gamma} \lambda_{\Gamma}^2 \sum_I T_{I, \Gamma} T_{I, \Gamma}^* m_I^0 , \quad (62)$$

$$\delta_{\sigma, \sigma'} n_{\sigma}^0 = \sum_{\Gamma} \lambda_{\Gamma}^2 \sum_{I(\sigma, \sigma' \in I)} f(\sigma, I \setminus \sigma) f(\sigma', I \setminus \sigma') T_{I \setminus \sigma, \Gamma} T_{I \setminus \sigma', \Gamma}^* m_I^0 . \quad (63)$$

Summary: Structure of the energy functional

In summary, we obtain the following Gutzwiller energy functional for the multi-band Hubbard models (12) in infinite dimensions

$$\begin{aligned} E^{\text{GA}} &= \sum_{i \neq j} \sum_{\sigma, \sigma', \gamma, \gamma'} t_{i, j}^{\gamma, \gamma'} q_{\gamma}^{\sigma} \left(q_{\gamma'}^{\sigma'} \right)^* \langle \hat{c}_{i, \sigma}^{\dagger} \hat{c}_{j, \sigma'} \rangle_{\Psi_0} + \sum_i \sum_{\sigma, \sigma' \in d} \epsilon_i^{\sigma, \sigma'} \langle \hat{c}_{i, \sigma}^{\dagger} \hat{c}_{i, \sigma'} \rangle_{\Psi_0} \\ &\quad + L \sum_{\Gamma} E_{\Gamma} \lambda_{\Gamma}^2 m_{\Gamma}^0 \end{aligned} \quad (64)$$

where, for the delocalised orbitals, the renormalisation factors are $q_{\gamma}^{\sigma} = \delta_{\sigma, \gamma}$. The single-particle state $|\Psi_0\rangle$ enters (64) solely through the non-interacting density matrix $\tilde{\rho}$ with the elements

$$\rho_{(i\sigma), (j\sigma')} \equiv \langle \hat{c}_{j, \sigma'}^{\dagger} \hat{c}_{i, \sigma} \rangle_{\Psi_0} . \quad (65)$$

Hence, the Gutzwiller energy functional simplifies to

$$E^{\text{GA}}(\tilde{\rho}, \lambda_{\Gamma}) = \sum_{i \neq j} \sum_{\sigma, \sigma', \gamma, \gamma'} t_{i, j}^{\gamma, \gamma'} q_{\gamma}^{\sigma} \left(q_{\gamma'}^{\sigma'} \right)^* \rho_{(j\sigma'), (i\sigma)} + \sum_{i; \sigma, \sigma' \in d} \epsilon_i^{\sigma, \sigma'} \rho_{(i\sigma), (i\sigma)} + L \sum_{\Gamma} E_{\Gamma} \lambda_{\Gamma}^2 m_{\Gamma}^0 . \quad (66)$$

It has to be minimised with respect to all elements of $\tilde{\rho}$ and the variational parameters λ_Γ obeying the constraints (62), (63) and

$$\tilde{\rho}^2 = \tilde{\rho} . \quad (67)$$

The latter constraint ensures that $\tilde{\rho}$ belongs to a single-particle product state.

There are several ways, how the constraints (62), (63) may be implemented in numerical calculations [10]. In this tutorial introduction, we will simply assume that Eqs. (62), (63) are solved by expressing some of the parameters λ_Γ by the remaining ‘independent’ parameters λ_Γ^i . Equation (67) is then the only remaining constraint in the minimisation of the resulting energy function $\bar{E}^{\text{GA}}(\tilde{\rho}, \lambda_\Gamma^i)$. If it is implemented by means of Lagrange parameters, see Appendix A, the minimisation with respect to $\tilde{\rho}$ leads to the effective single-particle Hamiltonian

$$\hat{H}_0^{\text{eff}} = \sum_{i \neq j} \sum_{\sigma, \sigma', \gamma, \gamma'} t_{i,j}^{\gamma, \gamma'} q_\gamma^\sigma (q_{\gamma'}^{\sigma'})^* \hat{c}_{i,\sigma}^\dagger \hat{c}_{j,\sigma'} + \sum_{i, \sigma \in d} \epsilon_i^{\sigma, \sigma'} \hat{c}_{i,\sigma}^\dagger \hat{c}_{i,\sigma} + \sum_{i, \sigma \in \ell} \eta_\sigma \hat{c}_{i,\sigma}^\dagger \hat{c}_{i,\sigma} \quad (68)$$

which gives us $|\Psi_0\rangle$ as the ground state of (68),

$$\hat{H}_0^{\text{eff}} |\Psi_0\rangle = E_0 |\Psi_0\rangle . \quad (69)$$

The ‘fields’ η_σ for the localised orbitals in (68) are given as [18]

$$\eta_\sigma = \frac{\partial}{\partial n_\sigma^0} \bar{E}^{\text{GA}}(\tilde{\rho}, \lambda_\Gamma^i) . \quad (70)$$

The remaining numerical problem is the solution of Eqs. (68)-(70) together with the minimisation condition

$$\frac{\partial}{\partial \lambda_\Gamma^i} \bar{E}^{\text{GA}}(\tilde{\rho}, \lambda_\Gamma^i) = 0 . \quad (71)$$

Numerical strategies to solve these equations have been discussed in detail in Ref. [10] to which we refer the interested reader.

Up to this point, the effective single-particle Hamiltonian (68),

$$\hat{H}_0^{\text{eff}} = \sum_{\mathbf{k}, \tau} E_{\mathbf{k}, \tau} \hat{h}_{\mathbf{k}, \tau}^\dagger \hat{h}_{\mathbf{k}, \tau} , \quad (72)$$

and its eigenvalues (‘band-energies’) $E_{\mathbf{k}, \tau}$ in momentum space are just auxiliary objects which determine $|\Psi_0\rangle$. One can readily show, however, that the non-interacting Fermi-surfaces, defined by the Fermi energy E_F ,

$$E_{\mathbf{k}, \tau} - E_F = 0 , \quad (73)$$

are equal to the correlated Fermi surfaces because the momentum distribution

$$n_{\mathbf{k}, \tau} \equiv \langle \hat{h}_{\mathbf{k}, \tau}^\dagger \hat{h}_{\mathbf{k}, \tau} \rangle_{\Psi_G} \quad (74)$$

has step discontinuities exactly at the momenta given by Eq. (73). The Fermi surface defined by (73) may therefore be compared to those, e.g., from de-Haas-van-Alphen experiments. Moreover, within a Landau-Fermi-liquid theory, the eigenvalues $E_{\mathbf{k}, \tau}$ turn out as the quasi-particle excitation energies which can be measured, e.g., in ‘angle-resolved photoemission spectroscopy’ (ARPES) experiments, see Refs. [9, 19].

3.3 Example: single-band Hubbard model

As a simple example we use the general results derived in Sec. 3.2, to recover the well-known Gutzwiller energy functional for the single-band Hubbard model [5]. For this model, the (local) Gutzwiller correlation operator (24) had the form

$$\hat{P} = \lambda_\emptyset \hat{m}_\emptyset + \lambda_\uparrow \hat{m}_\uparrow + \lambda_\downarrow \hat{m}_\downarrow + \lambda_d \hat{d}, \quad (75)$$

where

$$\hat{m}_\emptyset = (1 - \hat{n}_\uparrow)(1 - \hat{n}_\downarrow) = 1 - \hat{n}_\uparrow - \hat{n}_\downarrow + \hat{d}, \quad (76)$$

$$\hat{m}_s = \hat{n}_s(1 - \hat{n}_{\bar{s}}) = \hat{n}_s - \hat{d}, \quad (77)$$

$\bar{\uparrow} = \downarrow$, $\bar{\downarrow} = \uparrow$, and \hat{d} has been defined in Eq. (19). Equation (54) gives us the expectation value for the occupation of the four local eigenstates,

$$m_\emptyset \equiv \langle \hat{m}_\emptyset \rangle_{\Psi_G} = \lambda_\emptyset^2 (1 - n_\uparrow^0)(1 - n_\downarrow^0), \quad (78)$$

$$\hat{m}_s \equiv \langle \hat{m}_s \rangle_{\Psi_G} = \lambda_s^2 n_s^0 (1 - n_{\bar{s}}^0), \quad (79)$$

$$d \equiv \langle \hat{d} \rangle_{\Psi_G} = \lambda_d^2 n_\uparrow^0 n_\downarrow^0. \quad (80)$$

With these equations, we can replace the original variational parameters λ_\emptyset , λ_s , λ_d by their corresponding expectation values m_\emptyset , m_s , d . This simplifies the expressions for the constraints (62), (63) which then read

$$1 = m_\emptyset + m_\uparrow + m_\downarrow + d, \quad (81)$$

$$n_s^0 = m_s + d. \quad (82)$$

Note that the second constraint (82) simply ensures that the correlated and the uncorrelated (spin-dependent) particle numbers are equal,

$$\langle \hat{n}_s \rangle_{\Psi_G} = m_s + d = n_s^0 = \langle \hat{n}_s \rangle_{\Psi_0}. \quad (83)$$

Equations (81), (82) can be readily solved, e.g., by expressing m_\emptyset , m_s as functions of d ,

$$m_\emptyset = 1 - n_\uparrow^0 - n_\downarrow^0 + d, \quad (84)$$

$$m_s = n_s^0 - d. \quad (85)$$

In this way, the only remaining variational parameter is the average number of doubly-occupied lattice sites d .

Finally, we can evaluate the hopping renormalisation factors (61),

$$q_s^{s'}(d) = \delta_{s,s'} (\lambda_d \lambda_{\bar{s}} n_{\bar{s}}^0 + \lambda_s \lambda_\emptyset (1 - n_{\bar{s}}^0)) \quad (86)$$

$$= \delta_{s,s'} \frac{1}{\sqrt{n_s^0(1 - n_s^0)}} (\sqrt{m_{\bar{s}} d} + \sqrt{m_s m_\emptyset}), \quad (87)$$

where, in the second line, we have used Eqs. (78)-(80). In summary, we obtain the variational energy functional

$$\bar{E}^{\text{GA}}(d, \Psi_0) = \sum_{s=\uparrow,\downarrow} (q_s^s(d))^2 \sum_{i,j} t_{i,j} \langle \hat{c}_{i,s}^\dagger \hat{c}_{j,s} \rangle_{\Psi_0} + L U d \quad (88)$$

for the single-band Hubbard model (19) in the Gutzwiller approximation.

4 Applications

4.1 Ferromagnetism in a Two-Band Hubbard Model

Since Gutzwiller's ground-breaking work we know that the single-band energy functional (88) leads to ferromagnetic ground states only under very special circumstances, e.g., if the density of states has a sharp peak at the Fermi level and the Coulomb interaction is much larger than the band width. From this observation, we can already conclude that ferromagnetism, as it naturally appears in transition metals, is most probably related to the orbital degeneracy of the partially filled 3d-shell in these systems. Therefore, it is quite instructive to study ferromagnetic instabilities in a system with two orbitals, as a first step from the simple one-band model towards a realistic description of materials with partially filled 3d-shells.

A) Model Specification

We consider a Hubbard model with two degenerate e_g orbitals per site on a simple three-dimensional cubic lattice. The local (atomic) Hamiltonian for this system is given in equation (16). We include realistic hopping parameters for transition metal energy bands to the nearest and second-nearest neighbours in (13). This choice avoids pathological features in the energy bands, such as perfect nesting at half band filling. The single-particle part of the Hamiltonian (13) is easily diagonalised in momentum space and leads to a density of states $D_0(\varepsilon)$ that is shown as a function of the band filling in Fig. 2.

The case $n_\sigma = n_\sigma^0 = 0.29$ corresponds to a maximum in the density of states at the Fermi energy. For this band filling, we expect the strongest tendency towards ferromagnetism.

B) Variational Energy Functional

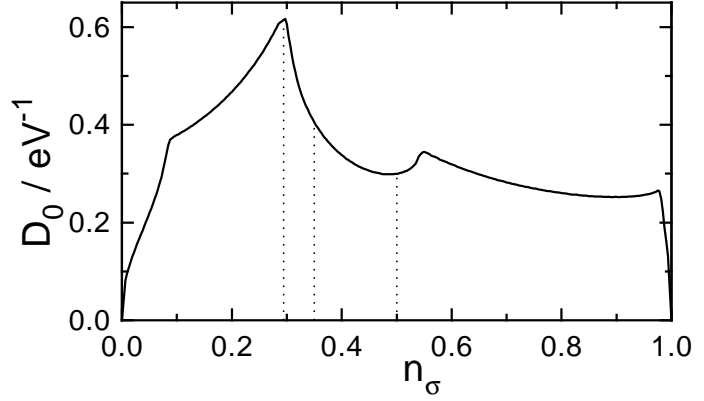
For a two-band model, it is still possible to give a manageable explicit expression of the energy as a function of the variational parameters. The eigenstates of the two-particle spectrum all belong to different representations of the point symmetry group, see table 1. Therefore, one can safely assume that the variational-parameter matrix $\lambda_{\Gamma, \Gamma'} = \delta_{\Gamma, \Gamma'}$ is diagonal and we have $\lambda_\Gamma = \lambda_{\Gamma'}$ for all states $|\Gamma\rangle, |\Gamma'\rangle$ that are degenerate due to the cubic symmetry. Then, we are left with 11 (independent) variational parameters $m_\Gamma = \lambda_\Gamma^2 m_\Gamma^0$:

- i) two parameters for an empty and a fully occupied site: m_\emptyset, f ;
- ii) four parameters for singly and triply occupied sites: m_s and t_s with $s = \uparrow, \downarrow$;
- iii) five parameters for doubly-occupied sites: $d_t^{\uparrow, \uparrow}, d_t^{\downarrow, \downarrow}, d_t^0$ (for the triplet 3A_2), d_E (for the doublet 1E), and d_A (for the singlet 1A_1).

For our degenerate two-band model, the uncorrelated local density matrix (31) is automatically diagonal and orbital independent,

$$\langle \hat{c}_{i,(b,s)}^\dagger \hat{c}_{i,(b',s')} \rangle_{\Psi_0} = \delta_{s,s'} \delta_{b,b'} n_s^0. \quad (89)$$

Fig. 2: Model density of states at the Fermi energy as a function of the orbital filling n_σ . The dashed lines indicate the half-filled case ($n_\sigma = 0.5$ and the fillings used in this section ($n_\sigma = 0.29$ and $n_\sigma = 0.35$). The total bandwidth is $W = 6.8$ eV.



As in the single-band case, the constraint equations (62), (63) can be solved explicitly, e.g., by considering the occupations

$$m_\emptyset = 1 - 2n_\uparrow^0 - 2n_\downarrow^0 + d_t^{\uparrow\uparrow} + d_t^{\downarrow\downarrow} + d_t^0 + d_A + 2d_E + 4t_\uparrow + 4t_\downarrow + 3f, \quad (90)$$

$$m_s = n_s^0 - \left[d_t^{ss} + t_{\bar{s}} + 2t_{\bar{s}} + f + \frac{1}{2} (d_A + 2d_E + d_t^0) \right] \quad (91)$$

as functions of the remaining nine independent parameters. The expectation value of the two-band Hubbard Hamiltonian is then given by

$$E_{\text{atom}}^{2b} = \sum_s (q_s^s)^2 \varepsilon_{s,0} + (U' - J)(d_t^{\uparrow\uparrow} + d_t^{\downarrow\downarrow} + d_t^0) + 2(U' + J)d_E + (U + J)d_A + (2U + 4U' - 2J)(t_\uparrow + t_\downarrow + f), \quad (92)$$

where we introduced the orbital-independent elements

$$q_s^s = \frac{1}{\sqrt{n_s^0(1 - n_s^0)}} \left[(\sqrt{t_s} + \sqrt{m_{\bar{s}}}) \frac{1}{2} (\sqrt{d_A} + 2\sqrt{d_E} + \sqrt{d_t^0}) + \sqrt{m_s} (\sqrt{m_\emptyset} + \sqrt{d_t^{ss}}) + \sqrt{t_{\bar{s}}} (\sqrt{d_t^{ss}} + \sqrt{f}) \right] \quad (93)$$

of the diagonal renormalisation matrix and the bare band energies

$$\varepsilon_{s,0} = \int_{-\infty}^{E_{F,s}} d\varepsilon \varepsilon D_0(\varepsilon). \quad (94)$$

For comparison, we will also consider the energy

$$E_{\text{dens}}^{(2b)} = \sum_s (\bar{q}_s^s)^2 \varepsilon_{s,0} + (U' - J)(d_1^{\uparrow\uparrow} + d_1^{\downarrow\downarrow}) + 2U'd_0 + 2Ud_c + (2U + 4U' - 2J)(t_\uparrow + t_\downarrow + f) \quad (95)$$

of a two-band model without the terms in the second line of the atomic Hamiltonian (16) since this is an approximation that is often made in studies on multi-band models. In this case, there are seven variational parameters $d_1^{\uparrow\uparrow}$, $d_1^{\downarrow\downarrow}$, d_0 , d_c , t_\uparrow , t_\downarrow , and f , which represent the occupation of

the configuration states $|I\rangle$. The probabilities for an empty site m_\emptyset and a singly-occupied site m_s are related to the variational parameters by

$$m_s = n_s^0 - [d_1^{ss} + t_{\bar{s}} + 2t_s + f + d_c + d_0] , \quad (96)$$

$$m_\emptyset = 1 - 2n_\uparrow^0 - 2n_\downarrow^0 + d_1^{\uparrow\uparrow} + d_1^{\downarrow\downarrow} + 2d_0 + 2d_c + 4t_\uparrow + 4t_\downarrow + 3f . \quad (97)$$

The renormalisation factors have the form

$$\begin{aligned} \bar{q}_s^s = \frac{1}{\sqrt{n_s^0(1-n_s^0)}} & \left[(\sqrt{t_s} + \sqrt{m_{\bar{s}}}) (\sqrt{d_c} + \sqrt{d_0}) \right. \\ & \left. + \sqrt{m_s} (\sqrt{m_\emptyset} + \sqrt{d_1^{ss}}) + \sqrt{t_{\bar{s}}} (\sqrt{d_1^{ss}} + \sqrt{f}) \right] . \end{aligned} \quad (98)$$

C) Ground-State Properties

The energies (92) and (95) have to be minimised with respect to their respective (nine or seven) independent variational parameters m_Γ and the magnetisation

$$M \equiv (n_\uparrow^0 - n_\downarrow^0)/2 , \quad (99)$$

for example, by means of the algorithm introduced in Ref. [10]. In Fig. 3 (left), the magnetisation M is shown as a function of U for fixed $J/U = 0.2$ ($U'/U = 0.6$). The critical interaction for the ferromagnetic transition, U_F^{atom} , is about a factor two larger than its value U_F^{HF} as obtained from the Hartree–Fock–Stoner theory. The corresponding values U_F^{dens} always lie somewhat below the values for the Gutzwiller wave function with full atomic correlations. In general, the relation $M_{\text{HF}}(U) > M_{\text{dens}}(U) > M_{\text{atom}}(U)$ holds, i.e., for all interaction strengths, the tendency to ferromagnetism is the strongest within the Hartree–Fock theory and weakest for Gutzwiller wave functions with atomic correlations. Furthermore, the slopes of $M(U)$ are much steeper in the Hartree–Fock results than in the presence of correlations.

The properties of the ferromagnetic phase strongly depend on the spectrum of the atomic two-electron configurations. To further analyse this point, we have included the case of $J_C = 0$, which changes only the excited two-electron states. A shift of the curve $M(U)$ results towards smaller interaction strengths; for a given magnetisation density, a smaller interaction strength is required as compared to the correct symmetry case $J = J_C$, see Fig. 3 (left). The effect is more pronounced when we go to the Gutzwiller wave function with pure density correlations. These results indicate that itinerant ferromagnetism is strongly influenced by the atomic multiplet spectra.

In Fig. 3 (left/a), we chose the particle density per band to be $n^0 = (n_\uparrow^0 + n_\downarrow^0)/2 = 0.29$, right at the maximum of the density of state curve, compare Fig. 2. In this case, there are finite slopes of the $M(U)$ curves at U_F , and a ‘Stoner criterion’ for the onset of ferromagnetism applies. In Fig. 3 (left/b), we chose the particle density per band as $n^0 = 0.35$. In this case, the density of states at the Fermi energy $D_0(E_{F,\uparrow}) + D_0(E_{F,\downarrow})$ first *increases* as a function of the magnetisation density. Therefore, a discontinuous transition thus occurs from the paramagnet to the ferromagnet.

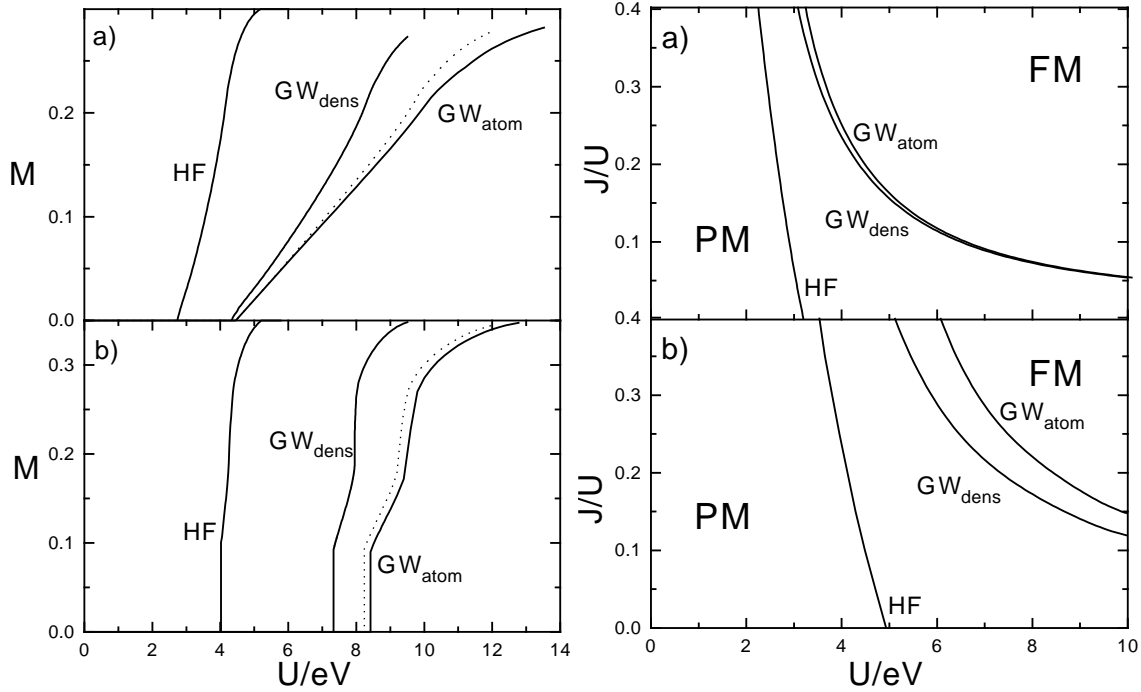


Fig. 3: Left: Magnetisation density per band as a function of U for the Hartree–Fock solution (HF), the Gutzwiller wave function with pure density correlations (GW_{dens}), and the Gutzwiller wave function with atomic correlations (GW_{atom}) for (a) $n_s = 0.29$ and (b) $n_s = 0.35$. The dotted line indicates the results for GW_{atom} with $J_C = 0$. The local exchange interaction is $J = 0.2U$ in all curves. Right: Phase diagram as a function of U and J for the Hartree–Fock solution (HF) and the two Gutzwiller wave functions (GW_{dens} , GW_{atom}) for (a) $n^0 = 0.29$ and (b) $n^0 = 0.35$; PM: paramagnet, FM: ferromagnet.

In the case of pure density correlations, a second jump in the $M(U)$ curve is observed that is absent in the other two curves. As discussed in Ref. [20], this jump is related to another feature of the density of states. In the Hartree–Fock theory, this feature is too weak to be of any significance in comparison to the interaction energy. When the full atomic correlations are taken into account, this first-order jump at a finite magnetisation density disappears due to the enhanced flexibility of the variational wave function.

Another remarkable difference between the Hartree–Fock and the Gutzwiller method lies in the approach to ferromagnetic saturation. In the Hartree–Fock theory, the magnetisation saturates at U values about 20% to 40% above the onset of ferromagnetism at U_F^{HF} . In contrast, in the variational approach saturation is reached at about twice the onset value, $U_{sat} \lesssim 2U_F$. However, even when the minority spin occupancies are zero and $\langle \hat{S}_z^{at} \rangle$ is constant, the majority spin occupancies s_\uparrow and $d_t^{\uparrow\uparrow}$ vary with U since the limit of zero empty sites is reached only for $U \rightarrow \infty$.

In Fig. 3 (right), we display the $J-U$ phase diagram for both fillings. It shows that the Hartree–Fock theory always predicts a ferromagnetic instability. In contrast, the correlated electron approach strongly supports the idea that a substantial on-site Hund’s rule exchange is required for the occurrence of ferromagnetism at realistic interaction strengths. For the case $n^0 = 0.29$,

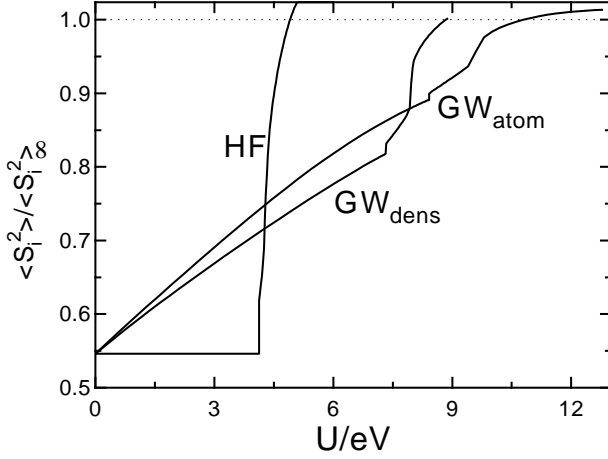


Fig. 4: Size of the local spin $\langle (\vec{S}_i)^2 \rangle$ as a function of the interaction strength for $J = 0.2U$ and band filling $n^0 = 0.35$ for the Hartree–Fock theory (HF) and the Gutzwiller wave functions (GW_{dens} , GW_{atom}).

the differences between the phase diagrams for the two correlated electron wave functions are minor. Due to the large density of states at the Fermi energy, the critical interaction strengths for the ferromagnetic transition are comparably small, and the densities for the double occupancies in both correlated wave functions do not differ much. For the larger band filling $n^0 = 0.35$, i.e., away from the peak in the density of state, the values for U_F are considerably larger and, in the atomic correlation case, the Gutzwiller wave functions can generate local spin triplets more easily while keeping the global paramagnetic phase.

The magnitude of the local spin as a function of U is shown in Fig. 4. For $U \rightarrow \infty$, each site is either singly occupied with probability $2 - 4n^0$ or doubly occupied (spin $S = 1$) with probability $4n^0 - 1$. Hence,

$$\langle (\vec{S}_i)^2 \rangle_\infty = (3/4)(2 - 4n^0) + 2(4n^0 - 1) = 5n^0 - 1/2. \quad (100)$$

For the correlated wave functions, this limit is reached from *above* since, for $U < \infty$, charge fluctuations first increase the number of spin-one sites at the expense of spin-1/2 sites, which turn into empty sites. A further decrease of U will also activate the singlet double occupancies and higher multiple occupancies. Thus, the local spin eventually reduces below $\langle (\vec{S}_i)^2 \rangle_\infty$. On the contrary, the Hartree–Fock theory does not give the proper large- U limit for the local spin. Instead, the Hartree–Fock limit is given by

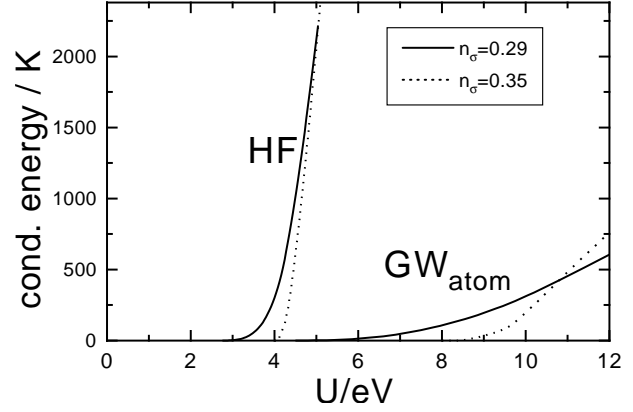
$$\langle (\vec{S}_i)^2 \rangle_\infty^{\text{HF}} = n^0(3 + 2n^0). \quad (101)$$

The change of $\langle (\vec{S}_i)^2 \rangle$ at U_F is only a minor effect within the correlated electron approach. In particular, this holds true for the case of atomic correlations, where about 90% of the local spin saturation value is already reached in the paramagnetic state. Again, the Hartree–Fock results are completely different. There, the local spin sharply increases as a function of the interaction strength since the absence of correlations fixes

$$\langle (\vec{S}_i)^2 \rangle^{\text{HF}}(U < U_F^{\text{HF}}) = \langle (\vec{S}_i)^2 \rangle(U = 0). \quad (102)$$

Finally, in Fig. 5, we display the energy differences between the paramagnetic and ferromagnetic ground states as a function of the interaction strength for $J = 0.1U$. For the correlated

Fig. 5: Condensation energy as a function of U for $J = 0.2U$ for the Hartree–Fock theory (HF) and the Gutzwiller wave function (GW_{atom}) for $n = 0.29$ (full lines) and $n = 0.35$ (dashed lines).



electron case, this quantity is of the order of the Curie temperature, which is in the range of 100 K – 1000 K in real materials. On the other hand, the Hartree–Fock theory yields small condensation energies only in the range of $U \approx 4$ eV; for larger U , the condensation energy is of order U . Including the correlation effects within the Gutzwiller theory, we have relatively small condensation energies even for interaction values as large as twice the bandwidth ($U \approx 10$ eV).

4.2 Antiferromagnetic order in iron-pnictide models

Since their recent discovery, the iron-based high- T_c superconductors, e.g., LaOFeAs, have attracted tremendous attention both in theory and experiment. From a theoretical point of view, these systems are of particular interest because their conduction electrons are less correlated than those of other high- T_c superconductors. In contrast to the cuprates, the pnictides' undoped parent compounds are antiferromagnetic metals at low temperatures, not insulators. However, the electronic mass is enhanced by a factor of two which indicates that electronic correlations are quite substantial in the pnictides, too.

The theoretical description of the pnictides' normal phases already turned out to be a difficult problem. Standard density-functional theory (DFT) grossly overestimates the size of their magnetic moment in the antiferromagnetic ground state. For example, in LaOFeAs experiment finds a staggered moment of $m = (0.4 \dots 0.8)\mu_B$ [21–23] whereas DFT calculations predict moments of $m \approx 1.8\mu_B$, or larger [24, 25]. For other pnictide compounds, the comparison is equally unfavourable.

The electronic structure of LaOFeAs near the Fermi energy is fairly two-dimensional and the bands are dominantly of iron d and (partially) of arsenic p character. A complete tight-binding model for LaOFeAs should therefore consist of eight bands (i.e., five iron d and three arsenic p bands) [26], see Fig. 6 (left). For many-particle approaches, however, the study of such an eight-band model is obviously quite challenging. Therefore, in many theoretical works on iron pnictides various simpler models have been proposed to study particular aspects of these materials. The fact that the bands near the Fermi energy are dominantly of iron d character suggest the study of an effective five-band model of pure iron d -bands. Such a model has been proposed, e.g., in Ref. [27], see Fig. 6 (middle). Even simpler models may be derived if one only aims to reproduce the Fermi surfaces of LaOFeAs. This is achieved, e.g., by the three-band

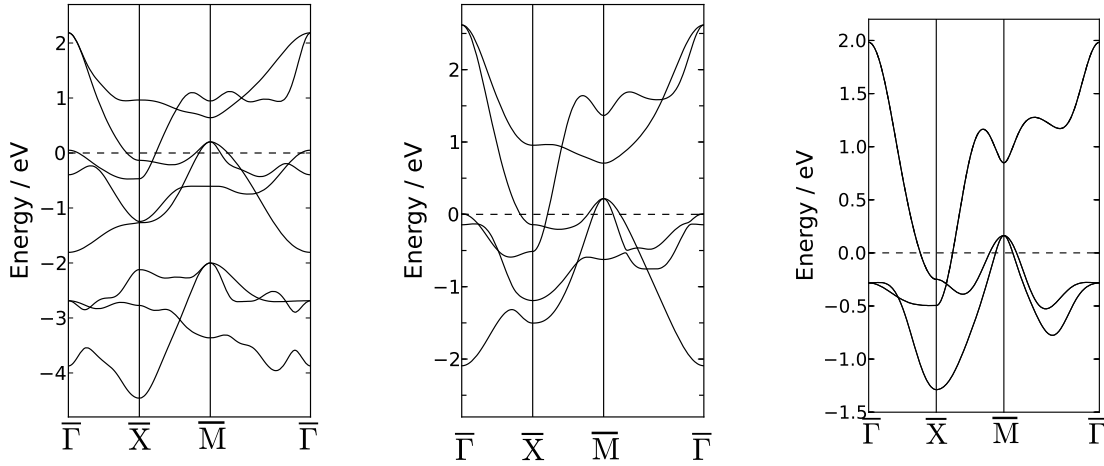


Fig. 6: Model band structures for LaOFeAs with eight bands [26] (left), five bands [27] (middle) and three bands [28] (right).

model in Fig. 6 (right), which was investigated in Ref. [28].

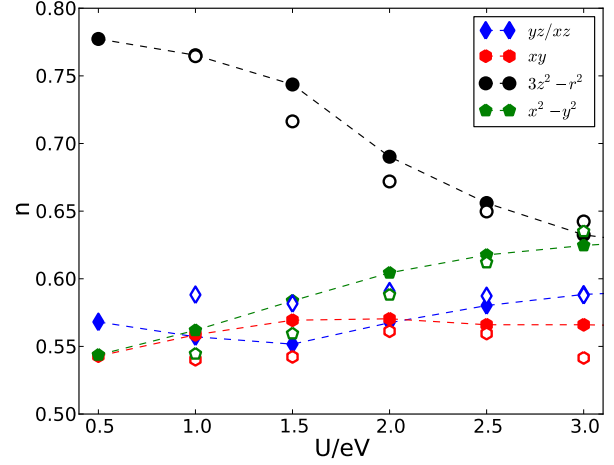
In cases where a simplified model reproduces certain properties of a material correctly, there will often remain doubts whether this agreement is merely coincidental or an indication that a model indeed captures the relevant physics of a system. A big advantage of the Gutzwiller theory is its numerical simplicity that allows one to study even complicated multi-band models with modest numerical efforts. In this way, it is possible to test the quality of simplified models by comparing their properties with those of more realistic Hamiltonians. In this section, we will compare the magnetic properties of all three models, displayed in Figs. 6. This comparison provides an interesting example of the dangers that lie in the study of ‘oversimplified’ model systems. Based on a Gutzwiller theory calculation it has been argued in Ref. [28] that the three-band model has a relatively small magnetic moment, in agreement with experiment. However, as we have shown in Ref. [29] the magnetic properties of the five-band model are very different from experiment and from those of the three-band model. One must therefore conclude that both models are insufficient in describing the magnetic properties of LaOFeAs. In fact, it turns out that an inclusion of the arsenic p orbitals is essential, see below.

In many theoretical studies, the following Hamiltonian for the Hubbard interaction $\hat{H}_{i;c}$ in (14) is used,

$$\begin{aligned}
 \hat{H}_c^{(1)} &= \hat{H}_c^{\text{dens}} + \hat{H}_c^{\text{sf}}, \\
 \hat{H}_c^{\text{dens}} &= \sum_{b,s} U(b,b) \hat{n}_{b,s} \hat{n}_{b',\bar{s}} + \sum_{b(\neq)b'} \sum_{s,s'} \tilde{U}_{s,s'}(b,b') \hat{n}_{b,s} \hat{n}_{b',s'}, \\
 \hat{H}_c^{\text{sf}} &= \sum_{b(\neq)b'} J(b,b') \left(\hat{c}_{b,\uparrow}^\dagger \hat{c}_{b,\downarrow}^\dagger \hat{c}_{b',\downarrow} \hat{c}_{b',\uparrow} + \text{h.c.} \right) + \sum_{b(\neq)b';s} J(b,b') \hat{c}_{b,s}^\dagger \hat{c}_{b',\bar{s}}^\dagger \hat{c}_{b,\bar{s}} \hat{c}_{b',s}.
 \end{aligned} \tag{103}$$

Here, we introduced $\tilde{U}_{s,s'}(b,b') = U(b,b') - \delta_{s,s'} J(b,b')$, where $U(b,b')$ and $J(b,b')$ are the local Coulomb and exchange interactions. For a system of five correlated d orbitals in cubic environment, however, the Hamiltonian (103) is incomplete [2]. The full Hamiltonian reads

Fig. 7: Orbital densities in Gutzwiller theory (full symbols) and in DMFT (open symbols) as a function of U (with $U/J = 4$) for the simplified local Hamiltonian $\hat{H}_c = \hat{H}_c^{(1)}$, see Eq. (103).



$\hat{H}_c = \hat{H}_c^{(1)} + \hat{H}_c^{(2)}$ where

$$\begin{aligned} \hat{H}_c^{(2)} = & \left[\sum_{t,s,s'} (T(t) - \delta_{s,s'} A(t)) \hat{n}_{t,s} \hat{c}_{u,s'}^\dagger \hat{c}_{v,s'} + \sum_{t,s} A(t) \left(\hat{c}_{t,s}^\dagger \hat{c}_{t,\bar{s}}^\dagger \hat{c}_{u,\bar{s}} \hat{c}_{v,s} + \hat{c}_{t,s}^\dagger \hat{c}_{u,\bar{s}}^\dagger \hat{c}_{t,\bar{s}} \hat{c}_{v,s} \right) \right. \\ & \left. + \sum_{t(\neq)t'(\neq)t''} \sum_{e,s,s'} S(t,t';t'',e) \hat{c}_{t,s}^\dagger \hat{c}_{t',s'}^\dagger \hat{c}_{t'',s'} \hat{c}_{e,s} \right] + \text{h.c.} \end{aligned} \quad (104)$$

Here, t and e are indices for the three t_{2g} orbitals with symmetries xy , xz , and yz , and the two e_g orbitals with symmetries $u = 3z^2 - r^2$ and $v = x^2 - y^2$. The parameters in (104) are of the same order of magnitude as the exchange interactions $J(b, b')$ and, hence, there is no a-priori reason to neglect them. Of all the parameters $U(b, b')$, $J(b, b')$, $A(t)$, $T(t)$, $S(t, t'; t'', e)$ only ten are independent in cubic symmetry. In a ‘spherical approximation’, i.e., assuming that all orbitals have the same radial wave-function, all parameters are determined by, e.g., the three Racah parameters A, B, C . We prefer to work with the orbital averages $J \propto \sum_{b \neq b'} J(b, b')$, and $U' \propto \sum_{b \neq b'} U(b, b')$ of the exchange and the inter-orbital Coulomb interaction. They are related to the intra-orbital interaction $U = U(b, b)$ via $U' = U - 2J$. Due to this symmetry relation, the three values of U, U' , and J do not determine the Racah parameters A, B, C uniquely. Therefore, we make use of the atomic relation $C/B = 4$ which is approximately satisfied in solids, too. In this way, the three Racah parameters and, consequently, all parameters in \hat{H}_c are functions of U and J . This permits a meaningful comparison of our results for all three model Hamiltonians.

In order to test the reliability of our approach we first compare our results for the partial densities of the five-band model with those from paramagnetic DMFT calculations. In Fig. 7 we show the density of electrons in each orbital as a function of U for fixed ratio $U/J = 4$. The full symbols give the Gutzwiller result for the simplified local Hamiltonian (103), $\hat{H} = \hat{H}_0 + \hat{H}_c^{(1)}$; open symbols give the DMFT results [30]. Obviously, the agreement between the Gutzwiller theory and DMFT is very good. This comes not as a surprise because both methods are derived in the limit of infinite spatial dimensions.

Figure 7 shows a common feature of multi-band model systems. The local Coulomb interaction induces a substantial charge flow between the bands because, for the local Coulomb interaction, it is energetically more favourable to distribute electrons equally among the bands. However,

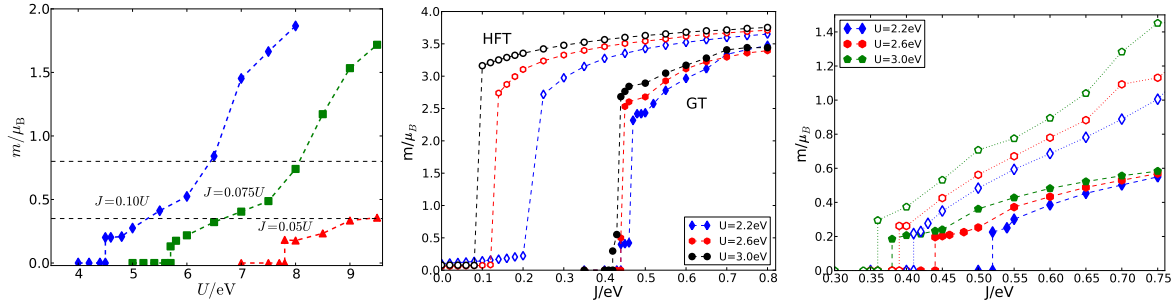


Fig. 8: Magnetic moment as a function of U for: left: model with eight bands [26]; middle: model with five bands [27] (Hartree–Fock and Gutzwiller theory); right: model with three bands [28] and local Hamiltonians \hat{H}_c^{dens} (dotted) and \hat{H}_c^{sf} (dashed).

the bands described by \hat{H}_0 are extracted from a DFT calculation whose predictions for the Fermi surface reproduce experimental data reasonably well. Therefore, the artificial charge flow as seen in Fig. 7 is clearly a consequence of the double counting of Coulomb interactions. Since the (paramagnetic) Fermi surface found in DFT reproduces its experimentally determined shape, we assume that the same holds for the paramagnetic orbital densities. For each value of the interaction parameters we therefore choose orbital on-site energies $\epsilon_i^{\sigma,\sigma}$ which lead to a paramagnetic ground state with the same orbital densities as in DFT. Note that a more sophisticated calculation of orbital densities requires the self-consistent Gutzwiller DFT scheme which we shall introduce in the following section.

In Figs. 8 we display the magnetic moment as a function of U for all three model systems. As mentioned before, the three-band model shows relatively small magnetic moments over a large range of Coulomb- and exchange interaction parameters, see Fig. 8 (right). This is in stark contrast to the results for the five-band model in Fig. 8 (middle). Here we find a transition to an antiferromagnet with a large moment, $m \gtrsim 2\mu_B$ which is as abrupt as in a corresponding Hartree–Fock calculation. However, if one takes into account the arsenic p bands, the magnetic moment is significantly smaller and in the range of experimental without the need of ‘fine-tuning’ the Coulomb- or exchange interaction parameters, see Fig. 8 (left). In summary, we can conclude that a proper understanding of the magnetic order in LaOFeAs requires the study of an eight-band model of iron d and arsenic p bands. It is possible, of course, that other properties of this compound, e.g., the superconducting order, may be correctly described by simpler model Hamiltonians.

5 The Gutzwiller density-functional theory

5.1 The Gutzwiller DFT equations

The model-based Gutzwiller method, which we have used in the previous section, ignores the fact that the hopping parameters (9) are actually functions of the density $n(\mathbf{r})$. Taking this functional dependence into account defines the ‘Gutzwiller density functional theory’ (GDFT). The explicit inclusion of the local Coulomb interaction within the Gutzwiller theory leads to

changes of the particle density $n(\mathbf{r})$ for three reasons:

i) The particle density $n(\mathbf{r})$ in the Gutzwiller-correlated ground state

$$n(\mathbf{r}) = \sum_{i \neq j} \sum_{\sigma, \sigma', \gamma, \gamma'} \phi_{i, \gamma}^*(\mathbf{r}) \phi_{j, \gamma'}(\mathbf{r}) q_{\gamma}^{\sigma} \left(q_{\gamma'}^{\sigma'} \right)^* \rho_{(j\sigma'), (i\sigma)} + \sum_i \sum_{\sigma} |\phi_{i, \sigma}(\mathbf{r})|^2 \rho_{(i\sigma), (i\sigma)} \quad (105)$$

differs from the corresponding DFT expression (10).

ii) Due to the renormalisation factors in (66) there will be an energy gain from changes of the hopping parameters $t_{i,j}^{\sigma, \sigma'} = t_{i,j}^{\sigma, \sigma'} \{n(\mathbf{r})\}$, which requires the re-adjustment of $n(\mathbf{r})$.

iii) The Coulomb interaction can lead to drastic changes of the occupation numbers $n_{i\sigma}^0 = \rho_{(i\sigma), (i\sigma)}$ in the localised orbitals, e.g., when the ground state is magnetically ordered. This also changes the non-local elements of the single-particle density matrix $\tilde{\rho}$ and the particle density (105).

These correlation-induced changes of the particle density are taken into account in the self-consistent GDFT by including the dependence of the hopping parameters on $n(\mathbf{r})$. Equation (105) shows that $n(\mathbf{r})$ and, consequently, $t_{i,j}^{\sigma, \sigma'}$ are unique functions of $\tilde{\rho}$ and λ_{Γ} . Therefore, the GDFT energy functional has the form

$$E^{\text{GDFT}}(\tilde{\rho}, \lambda_{\Gamma}) = \sum_{\sigma, \sigma', \gamma, \gamma'} q_{\gamma}^{\sigma} \left(q_{\gamma'}^{\sigma'} \right)^* \sum_{i \neq j} t_{i,j}^{\gamma, \gamma'}(\tilde{\rho}, \lambda_{\Gamma}) \rho_{(j\sigma'), (i\sigma)} + \sum_{i, \sigma \in d} \epsilon_i^{\sigma, \sigma} \rho_{(i\sigma), (i\sigma)} + L \sum_{\Gamma} E_{\Gamma} \lambda_{\Gamma}^2 m_{\Gamma}^0. \quad (106)$$

We assume again that the constraints (62), (63) are solved by expressing some of the parameters λ_{Γ} by the remaining ‘independent’ parameters λ_{Γ}^i . The resulting energy functional $\bar{E}^{\text{GDFT}}(\tilde{\rho}, \lambda_{\Gamma}^i)$ has to be minimised with respect to the density matrix $\tilde{\rho}$ and the independent variational parameters λ_{Γ}^i ,

$$\frac{\partial}{\partial \rho_{(i\sigma), (j\sigma')}} \bar{E}^{\text{GDFT}}(\tilde{\rho}, \lambda_{\Gamma}^i) = 0 \quad , \quad \frac{\partial}{\partial \lambda_{\Gamma}^i} \bar{E}^{\text{GDFT}}(\tilde{\rho}, \lambda_{\Gamma}^i) = 0, \quad (107)$$

with the usual constraint (67) for the non-interacting density matrix $\tilde{\rho}$. The minimisation with respect to $\tilde{\rho}$ leads to ‘renormalised’ Kohn–Sham equations of the form (8), (9), (11), and (105) with Eq. (8) replaced by

$$\hat{H}_0 = \sum_{i \neq j} \sum_{\sigma, \sigma', \gamma, \gamma'} q_{\gamma}^{\sigma} \left(q_{\gamma'}^{\sigma'} \right)^* t_{i,j}^{\gamma, \gamma'}(\tilde{\rho}, \lambda_{\Gamma}) \hat{c}_{i, \sigma}^{\dagger} \hat{c}_{j, \sigma'} + \sum_{i, \sigma \in \ell} \eta_{\sigma} \hat{c}_{i, \sigma}^{\dagger} \hat{c}_{i, \sigma} \quad (108)$$

and by [18]

$$\eta_{\sigma} \equiv \frac{1}{L} \sum_{\sigma, \sigma', \gamma, \gamma'} \left[\frac{\partial}{\partial n_{\sigma}} q_{\gamma}^{\sigma} \left(q_{\gamma'}^{\sigma'} \right)^* \right] \sum_{i \neq j} t_{i,j}^{\gamma, \gamma'}(\tilde{\rho}, \lambda_{\Gamma}) \rho_{(j\sigma'), (i\sigma)} + \frac{\partial}{\partial n_{\sigma}} \sum_{\Gamma} E_{\Gamma} \lambda_{\Gamma}^2 m_{\Gamma}^0, \quad (109)$$

respectively. The set of Eqs. (9), (105), and (106)-(109), which have to be solved self-consistently, constitute the GDFT. This approach was first proposed in Refs. [31–33] and has been applied

to various systems in Refs. [32–36]. In all these works, the authors report a remarkably better agreement with experiment than it could be obtained by a model-based Gutzwiller calculation for the same materials.

One of the main advantages of the DFT is its ‘ab-initio’ character, i.e., the absence of any adjustable parameters. Unfortunately, this benefit of the DFT cannot be fully maintained in the GDFT because that would require the calculation of the two-particle interaction parameters $U_i^{\sigma_1, \sigma_2, \sigma_3, \sigma_4}$ in the localised orbitals from first principles. The straightforward *ab-initio* solution of this problem, namely to calculate these parameters from the Wannier orbitals $\phi_{i, \sigma}(\mathbf{r})$, is known to yield values which are much too large. Apparently, screening effects decrease the Coulomb-interaction parameters significantly. These effects, however, are not well understood and a quantitatively reliable technique for the calculation of screened Coulomb parameters does not exist. For this reason one usually applies the same strategy as in model-based calculations where the matrix elements $U_i^{\sigma_1, \sigma_2, \sigma_3, \sigma_4}$ are somehow parameterised, e.g., in spherical approximation by means of a few Racah parameters. These are chosen to obtain the best agreement with experiment. In this context, it is a big advantage that the GDFT provides one with more data, e.g., with structural properties, that can be compared to experiment, see Sec. 5.2.

As mentioned before, the local Coulomb interaction appears twice in the Hamiltonian (14) because it also affects the on-site energies $\epsilon_i^{\sigma, \sigma'}$. There are several ways to overcome this ‘double-counting problem’ which have been proposed in the literature, see, e.g., Ref. [37]. According to Refs. [32–36], the subtraction of the mean-field operator

$$\hat{H}_{\text{dc}} = 2 \sum_{\sigma, \sigma', \gamma \in \ell} (U_i^{\sigma, \gamma, \gamma, \sigma'} - U_i^{\gamma, \sigma, \gamma, \sigma'}) n_{\gamma}^0 \hat{c}_{i, \sigma}^{\dagger} \hat{c}_{i, \sigma'} \quad (110)$$

from $\hat{H}_{i; \text{c}}$ leads to good results within the GDFT.

5.2 Application

As an example for the relevance of the GDFT we show results on the iron-pnictides LaOFeAs and BaFe₂As₂ which have been presented in Ref. [35]. The failure to describe the magnetic order is not the only problem the DFT faces in its calculations on iron-pnictides. There are also substantial deviations between the experimental results and DFT predictions on lattice parameters, in particular for the distance between Fe and As. Taking correlations into account more properly, as it is done within the GDFT, changes these lattice parameters significantly. Figure 9 shows the interlayer distance d_{FeAs}^z as a function of J for several values of U . In both systems, the exchange interaction clearly plays an important role and needs to be included in order to reproduce the experimental value for d_{FeAs}^z . As a consequence, other properties are also changed significantly as a function of J , see Ref. [35]. It should be noted that the calculations in Ref. [35] were carried out with the simplified local Hamiltonian \hat{H}_c^{dens} in Eq. (103). Taking the full atomic interaction into account may therefore change results, at least quantitatively. Nevertheless, these results already illustrate how important it is, in studies on transition metal compounds, to treat the local Coulomb interaction in a more sophisticated way than provided by state-of-art DFT methods.

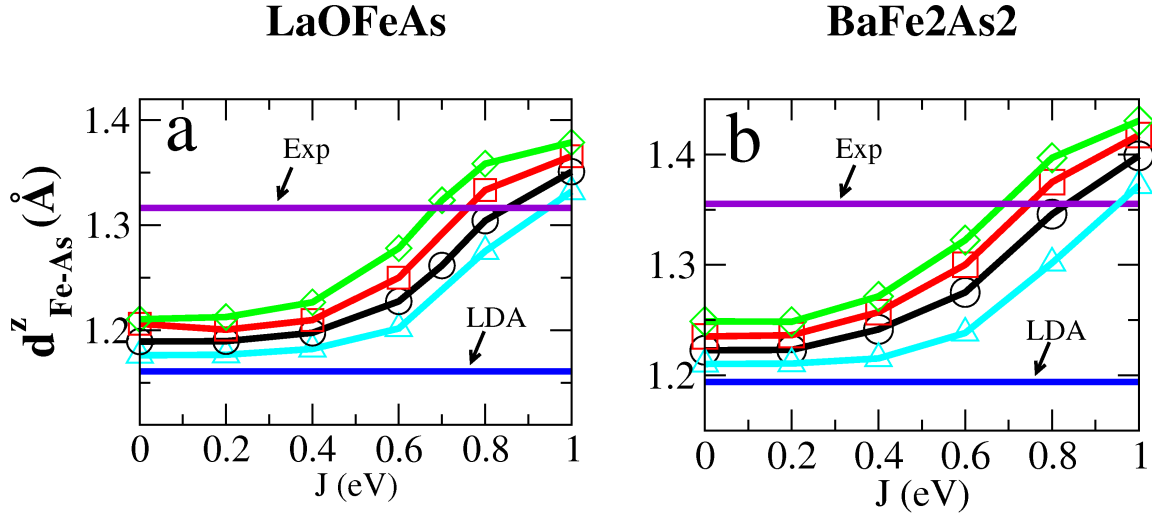


Fig. 9: Interlayer distance d_{FeAs}^z in LaOFeAs and BaFe₂As₂ as a function of J for several values of U .

6 Summary and Outlook

In this tutorial presentation, we have provided a comprehensive introduction into the Gutzwiller variational approach and its merger with the density functional theory. Numerically, the Gutzwiller method is rather ‘cheap’ as compared to other many-particle approaches. It will therefore, quite likely, emerge as an important tool for the improvement of existing ab-initio methods. There are two more recent developments which we shall briefly mention as an outlook:

- **The time-dependent Gutzwiller theory**

The Gutzwiller theory, as introduced in this presentation, can be used for the calculation of ground-state properties and of quasi-particle energies in the Fermi-liquid regime. For the description of experiments one often needs to calculate two-particle response functions such as the magnetic susceptibility or the optical conductivity. This is achieved by the so-called ‘time dependent Gutzwiller theory’. This method is derived in a very similar way as the ‘random-phase approximation’ can be introduced as a time-dependent generalisation of the Hartree–Fock theory. It was first developed for single-band Hubbard models by Seibold et al. [38, 39] and has been applied with astonishing success to quite a number of such models and response functions [40–50]. Recently, the method has been generalised for the study of multi-band models [51, 52].

- **Beyond the Gutzwiller approximation**

As we have demonstrated in this presentation, the energy-functional which we derived in infinite dimensions (i.e., the Gutzwiller approximation), constitutes already a major improvement over, e.g., the Hartree–Fock theory. It is well-known, however, that the limit of infinite spatial dimensions has some severe limitations. For example, if we consider the Fermi surface of a single-band Hubbard model, it will be independent of U as long as

no symmetry-broken phases are considered. This cannot be correct in finite dimensions which becomes evident already from straightforward perturbation theory in U [53]. It is also known from a numerical evaluation of Gutzwiller wave functions in two dimensions that, for sufficiently large values of U , the variational ground states can be superconducting [54, 55]. This is also not reproduced within the Gutzwiller approximation. In a recent work, we have therefore proposed an efficient diagrammatic method for the evaluation of Gutzwiller wave functions in finite dimensions [56]. It has enabled us to study correlation-induced Fermi-surface deformations [56] as well as superconductivity (unpublished). The numerical efforts of this method are still moderate and the investigation of more complicated multi-band models will therefore be feasible in the near future.

Acknowledgement

The proofreading of this manuscript by F. Gebhard is gratefully acknowledged. I also thank the authors of Ref. [35] for providing me with the data, shown in Fig. 9.

Appendix

A Minimisation of functions with respect to non-interacting density matrices

We consider a general function $E(\tilde{\rho})$ of a non-interacting density matrix $\tilde{\rho}$ with the elements

$$\rho_{\gamma,\gamma'} = \langle \hat{c}_{\gamma'}^\dagger \hat{c}_\gamma \rangle_{\Phi_0} . \quad (111)$$

The fact that $\tilde{\rho}$ is derived from a single-particle product wave function $|\Phi_0\rangle$ is equivalent to the matrix equation $\tilde{\rho}^2 = \tilde{\rho}$. Hence, the minimum of $E(\tilde{\rho})$ in the ‘space’ of all *non-interacting* density matrices is determined by the condition

$$\frac{\partial}{\partial \rho_{\gamma',\gamma}} L(\tilde{\rho}) = 0 , \quad (112)$$

where we introduced the ‘Lagrange functional’

$$L(\tilde{\rho}) \equiv E(\tilde{\rho}) - \sum_{l,m} \Omega_{l,m} [\tilde{\rho}^2 - \tilde{\rho}]_{m,l} \quad (113)$$

$$= E(\tilde{\rho}) - \sum_{l,m} \Omega_{l,m} \left(\sum_p \rho_{m,p} \rho_{p,l} - \rho_{m,l} \right) \quad (114)$$

and the matrix $\tilde{\Omega}$ of Lagrange parameters $\Omega_{l,m}$. The minimisation of (113) leads to the matrix equation

$$\tilde{H} = \tilde{\rho} \tilde{\Omega} + \tilde{\Omega} \tilde{\rho} - \tilde{\Omega} \quad (115)$$

for the ‘Hamilton matrix’ \tilde{H} with the elements

$$H_{\gamma,\gamma'} = \frac{\partial}{\partial \rho_{\gamma',\gamma}} E(\tilde{\rho}) . \quad (116)$$

For density matrices which satisfy $\tilde{\rho}^2 = \tilde{\rho}$, Eq. (115) leads to $[\tilde{H}, \tilde{\rho}] = 0$. Hence, \tilde{H} and $\tilde{\rho}$ must have the same basis of (single-particle) eigenvectors and, consequently, $|\Phi_0\rangle$ is the ground state of

$$\hat{H}_0^{\text{eff}} = \sum_{\gamma, \gamma'} H_{\gamma, \gamma'} \hat{c}_\gamma^\dagger \hat{c}_{\gamma'} . \quad (117)$$

References

- [1] P. Hohenberg and W. Kohn. *Phys. Rev.*, 136:864, 1964.
- [2] S. Sugano, Y. Tanabe, and H. Kamimura. *Multiplets of Transition-Metal Ions in Crystals*. Pure and Applied Physics 33, Academic Press, New York, 1970.
- [3] E. Feenberg. *Theory of Quantum Liquids*. Academic Press, New York, 1969.
- [4] B. E. Clements, E. Krotscheck, J. A. Smith, and C. E. Campbell. *Phys. Rev. B*, 47:5239, 1993.
- [5] M.C. Gutzwiller. *Phys. Rev. Lett*, 10:159, 1963.
- [6] M.C. Gutzwiller. *Phys. Rev.*, 134:A923, 1964.
- [7] M.C. Gutzwiller. *Phys. Rev.*, 137:A1726, 1965.
- [8] J. Bünnemann, W. Weber, and F. Gebhard. *Phys. Rev. B*, 57:6896, 1998.
- [9] J. Bünnemann, F. Gebhard, and W. Weber. In A. Narlikar, editor, *Frontiers in Magnetic Materials*. Springer, Berlin, 2005.
- [10] J. Bünnemann, T. Schickling, F. Gebhard, and W. Weber. *physica status solidi (b)*, 249:1282, 2012.
- [11] J. Bünnemann, K. Jávorné-Radnóczy, P. Fazekas, and F. Gebhard. *J. Phys. Cond. Matt*, 17:3807, 2005.
- [12] W. Metzner and D. Vollhardt. *Phys. Rev. B*, 37:7382, 1988.
- [13] M. Kollar and D. Vollhardt. *Phys. Rev. B*, 65:155121, 2002.
- [14] F. Gebhard and D. Vollhardt. *Phys. Rev. Lett.*, 59:1472, 1987.
- [15] F. Gebhard and D. Vollhardt. *Phys. Rev. B*, 38:6911, 1988.
- [16] F. Gebhard. *Phys. Rev. B*, 41:9452, 1990.
- [17] J. Bünnemann. *Eur. Phys. J. B*, 4:29, 1998.
- [18] Note that, in general, the fields η_σ are non-diagonal ($\eta_{\sigma,\sigma'}$) and given as the derivative of the energy-functional with respect to the elements of the non-interacting density matrix (30). This requires the evaluation of the more complicated energy functional without the condition (31), see Ref. [10].
- [19] J. Bünnemann, F. Gebhard, and R. Thul. *Phys. Rev. B*, 67:75103, 2003.
- [20] J. Bünnemann and W. Weber. *Physica B*, 230:412, 1997.

- [21] C. de la Cruz, Q. Huang, J. W. Lynn, J. Li, W. Ratcliff, J. L. Zarestky, H. A. Mook, G. F. Chen, J. L. Luo, N. L. Wang, and P. Dai. *Nature London*, 453:899, 2008.
- [22] N. Qureshi, Y. Drees, J. Werner, S. Wurmehl, C. Hess, R. Klingeler, B. Büchner, M. T. Fernández-Díaz, and M. Braden. *Phys. Rev. B*, 82:184521, 2010.
- [23] H. F. Li, H.-F. Li, W. Tian, J.-Q. Yan, J. L. Zarestky, R. W. McCallum, T. A. Lograsso, and D. Vaknin. *Phys. Rev. B*, 82:064409, 2010.
- [24] E. I. Mazin, M. D. Johannes, L. Boeri, K. Koepernik, and D. J. Singh. *Phys. Rev. B*, 78:085104, 2008.
- [25] Y.-Z. Zhang, I. Opahle, H. O. Jeschke, and R. Valentí. *Phys. Rev. B*, 81:094505, 2010.
- [26] O. K. Andersen and L. Boeri. *Ann. Physik (Berlin)*, 523:8, 2011.
- [27] S. Graser, T. Maier, P. Hirschfeld, and D. Scalapino. *New Journal of Physics*, 11:025016, 2009.
- [28] S. Zhou and Z. Wang. *Phys. Rev. Lett.*, 105:096401, 2010.
- [29] T. Schickling, F. Gebhard, and J. Bünemann. *Phys. Rev. Lett.*, 106:146402, 2011.
- [30] H. Ishida and A. Liebsch. *Phys. Rev. B*, 81:054513, 2010.
- [31] K. M. Ho, J. Schmalian, and C. Z. Wang. *Phys. Rev. B*, 77:073101, 2008.
- [32] X. Deng, X. Dai, and Z. Fang. *Europhys. Lett.*, 83:37008, 2008.
- [33] X. Deng, L. Wang, X. Dai, and Z. Fang. *Phys. Rev. B*, 79:075114, 2009.
- [34] G. Wang, X. Dai, and Z. Fang. *Phys. Rev. Lett.*, 101:066403, 2008.
- [35] G. Wang, Y. M. Qian, G. Xu, X. Dai, and Z. Fang. *Phys. Rev. Lett.*, 104:047002, 2010.
- [36] H. Weng, G. Xu, H. Zhang, S.-C. Zhang, X. Dai, and Z. Fang. *Phys. Rev. B*, 84:060408, 2011.
- [37] M. Karolak, G. Ulm, T. Wehling, V. Mazurenko, A. Poteryaev, and A. Lichtenstein. *Journal of Electron Spectroscopy and Related Phenomena*, 181:11, 2010.
- [38] G. Seibold, E. Sigmund, and V. Hizhnyakov. *Phys. Rev. B*, 57:6937, 1998.
- [39] G. Seibold and J. Lorenzana. *Phys. Rev. Lett.*, 86:2605, 2001.
- [40] G. Seibold. *Phys. Rev. B*, 58:15520, 1998.
- [41] G. Seibold, F. Becca, and J. Lorenzana. *Phys. Rev. B*, 67:085108, 2003.
- [42] J. Lorenzana and G. Seibold. *Phys. Rev. Lett.*, 90:066404, 2003.

- [43] G. Seibold and J. Lorenzana. *Phys. Rev. B*, 69:134513, 2004.
- [44] G. Seibold, F. Becca, P. Rubin, and J. Lorenzana. *Phys. Rev. B*, 69:155113, 2004.
- [45] J. Lorenzana, G. Seibold, and R. Coldea. *Phys. Rev. B*, 72:224511, 2005.
- [46] G. Seibold and J. Lorenzana. *Phys. Rev. Lett.*, 94:107006, 2005.
- [47] G. Seibold and J. Lorenzana. *Phys. Rev. B*, 73:144515, 2006.
- [48] G. Seibold and J. Lorenzana. *Journal of Superconductivity and Novel Magnetism*, 20:619, 2007.
- [49] G. Seibold, F. Becca, and J. Lorenzana. *Phys. Rev. Lett.*, 100:016405, 2008.
- [50] G. Seibold, F. Becca, and J. Lorenzana. *Phys. Rev. B*, 78:045114, 2008.
- [51] E. v. Oelsen, G. Seibold, and J. Bünemann. *Phys. Rev. Lett.*, 107:076402, 2011.
- [52] E. v. Oelsen, G. Seibold, and J. Bünemann. *New J. Phys.*, 13:113031, 2011.
- [53] C. J. Halboth and W. Metzner. *Z. Phys. B*, 102:501, 1997.
- [54] D. Eichenberger and D. Baeriswyl. *Phys. Rev. B*, 76:180504, 2007.
- [55] D. Eichenberger and D. Baeriswyl. *Phys. Rev. B*, 79:100510, 2009.
- [56] J. Bünemann, T. Schickling, and F. Gebhard. *Europhys. Lett.*, 98:27006, 2012.